DISSERTATION

Mechanisms of chemical-induced degeneration of monoaminergic neurons

(化学物質によるモノアミン作動性神経変性のメカニズム)

September, 2023

Graduated School of Pharmaceutical Science
Tokyo University of Science

Alzahraa Ahmed Mohamed Ibrahim Fergany

GENERAL ABSTRACT

People are exposed to variety of environmental electrophiles such as acrylamide (ACR) in baked foods, methylmercury accumulated in fish, cadmium in rice, aromatic hydrocarbon quinones formed during gasoline combustion or crotonaldehyde in tobacco smoke. The mechanism how these electrophiles induce toxicity is thought to modify nucleophilic functions in proteins, such as cysteine residues, forming adducts and activating cellular redox signal transduction pathways such as kinases and transcription factors. Higher concentrations of electrophiles, on the other hand, disrupt such signaling by nonselective covalent modification of cellular proteins leading to eventually oxidative and inflammatory response which may be the cause of the neurotoxicity and or neurodegeneration. This work focus on the ACR and (B[a]P) neurotoxicity in mice.

Acrylamide (ACR) is, a white, odorless, and water-soluble substance, a soft electrophile which is known as a potent neurotoxicant in humans. It is generated during processing food at high temperatures through the Maillard reaction. There are different sources of ACR including fried, baked potatoes, coffee and bakery products contain substantial amounts of acrylamide. It is also used in water sanitation and production flocculators, grouts, and press fabrics. Besides, chemical monomer acrylamide is used to produce polymer compounds that are utilized to make plastic, sheets, adhesive tapes, colors, and food packaging. Therefore, humans are exposed to ACR through different sources in addition to occupationally exposure. In humans and experimental animals, acrylamide is a known neurotoxicant that causes neuropathies and encephalopathies. Inflammatory cytokines play an important role in the inflammatory response of the body against stress, damage, or disease. One of the important proinflammatory cytokines is interleukin-1β (*IL-1β).* It is secreted from microglia and considered a critical neuroinflammatory component of brain reaction to any insults, but its role in electrophile-induced neurotoxicity is not well understood.

Benzo[a]pyrene (B[a]P) is the most common polycyclic aromatic hydrocarbon (PAH) found in the atmosphere, surface water, soil, and sediments. It is present in cigarette smoke as well as food products, particularly when smoked and grilled, so humans are exposed to B[a]P from multiple sources. B[*a*]P and other PAHs have been shown to be formed during the burning of fossil fuels, wood, and other organic materials. B[*a*]P has been detected at high levels in cigarette smoke, diesel exhaust, charcoal-based foods, as well as industrial wastes. The main sources of human B[*a*]P exposure are contaminated food and the air. Occupational exposure also to B[*a*]P, occurs mainly through inhalation or dermal absorption through combustion of PAHs mixture at workplaces. There are several studies demonstrating that these electrophiles act through increase in ROS formation and induced imbalance

in the biological oxidant to antioxidant ratio leading to oxidative stress and alteration of antioxidant defense system which causes subsequently DNA damage or neurological impairments such as neuronal loss, glial activation or neuroinflammation.

This thesis aims to clarify the mechanisms which may be the cause of neurotoxicity or neurodegeneration caused by environmental electrophiles. The first study aims to investigate the role of *IL-1β* in ACR-induced neurotoxicity in mice as *IL-1β* one of cytokines that released in response to any harmful stimuli to relive inflammatory response. The second study aims to investigate the underlying mechanisms and histopathological changes in mouse brain in relation to B[*a*]P-induced neurotoxicity in mice.

In the first study, Ten-week-old male wild-type and *IL-1β* knock-out mice (C57BL/6JJmsSLC) were allocated into three groups each (n=10) and exposed to acrylamide at 0, 12.5, 25 mg/kg body weight by oral gavage for 28 days. Compared to wild-type mice, the results showed a significant increase in landing foot spread test and a significant decrease in density of cortical noradrenergic axons in *IL-1β* KO mice exposed to acrylamide at 25mg/kg bw. Exposure to acrylamide at 25mg/kg significantly increased cortical gene expression of *Gclc* , *Gpx1* and *Gpx4* in wild-type mice but decreased them in *IL-1β* KO mice. The same exposure level significantly increased total glutathione and oxidized glutathione (GSSG) in the cerebellum of wild-type mice but neither changed total glutathione nor decreased GSSG in the cerebellum of *IL-1β* KO mice. The basal level of malondialdehyde in the cerebellum was higher in *IL-1β* KO mice than in wild-type mice. The results suggest that IL-1β protects the mouse brain against acrylamide-induced neurotoxicity, probably through suppression of oxidative stress by glutathione synthesis and peroxidation. This unexpected result provides new insight on the protective role of IL-1β in acrylamide-induced neurotoxicity.

In the second study, 48 wild-type male mice (10 weeks of age) were allocated into 4 groups and exposed to B[a]P at 0, 2.88, 8.67 or 26.00 μg/mice, which is approximately equivalent to 0.12, 0.37 and 1.12 mg/kg bw, respectively, by pharyngeal aspiration once/week for 4 weeks. The density of noradrenergic and serotonergic axons was evaluated by immunohistochemistry in the hippocampal CA1 and CA3 areas. Exposure to B[a]P at 2.88 μg/mice or more decreased the density of noradrenergic or serotonergic axons in the CA1 area and the density of noradrenergic axons in the CA3 area in the hippocampus of mice. Furthermore, exposure to B[a]P dose-dependently upregulated *Tnfα* at 8.67 μg/mice or more, as well as upregulating *Il-1β* at 26 μg/mice, *Il-18* at 2.88 and 26 μg/mice and *Nlrp3* at 2.88 μg/mice. The results demonstrate that exposure to B[a]P induces degeneration of noradrenergic

or serotonergic axons and suggest the involvement of proinflammatory or inflammation-related genes with B[a]P- induced neurodegeneration.

Key Words: Acrylamide, Benzo[a]pyrene, *IL-1β,* Neurotoxicity; Noradrenergic axons, Serotonergic axon, Neuroinflammation.

DEDICATION

This thesis is dedicated to the sake of Allah, my creator and my master who give me the strength to finish this work, my great teacher and messenger, Mohamed (May Allah bless and grant him, who taught us the purpose of life). My parents who always encouraged me with their heartful words through this work. My beloved sisters (Alrabab Fergany and Aisha Fergany) and my brothers (Abdallah Fergany and Ahmed Tarek), who always give me the strength with kind words to fulfil this work.

ACKNOWLEDGMENT

This work carried on the department of Occupational and Environmental health, Graduated school of Pharmaceutical Science, Tokyo University of Science, Noda, within the fiscal year 2020-2023. First and foremost, praises and thanks to the God, the Almighty, for His showers of blessings throughout my research work to complete the research successfully. I would like to acknowledge the financial support provided by MEXT Scholarships, the Japan government's scholarship program, for letting me be part of this incredible leaders' network.

I would like to express my deep and sincere gratitude to my supervisor Prof. Gaku Ichihara for giving me the opportunity to carry out my research in his lab and providing invaluable guidance throughout this research. His dynamism, vision, sincerity, and motivation have deeply inspired me. It was a great privilege and honor to work and study under his guidance. I am extremely grateful for what he has offered me. I would also like to thank him for his friendship, empathy, and patience. I am extending my heartfelt thanks to Prof. Sahoko Ichihara, who always help me through her directions and guidance in this research.

Very special thanks for Ms. Satoko Arai, through her support with excellent secretarial work through whole my stay in Japan and her support for Japanese language translation in work and any personal issue.

My sincere thanks also goes to Dr. Cai Zong, who always help, support, and direct me towards the correct way to perform my experiment. Besides his encouragement, insightful comments, and data analysis to get this thesis perfectly.

I would like to express my special thanks To Dr. Fredrick Ekuban for his kind help, support, and directions through whole my experiment and his patience to explain every detail on the techniques to carry out my experiment in correct way.

Special thanks go to all members of Ichihara lab Mr. Yusuke Kimura, Dr. Abigil Ekuban, Ms. Aina Suzuki, Ms. Kyoka Yamazaki, Ms. Haru Sato, whom I had the opportunity to work with them closely and I learned from them too much. I am very thankful for all of you, and I appreciate your kind friendship through my Research work.

I am extending my thanks to all the members of Genetics and Genetic Engineering laboratory at Faculty of Veterinary Medicine, Alexandria University, Egypt.

I am extremely grateful to my parents for their love, prayers, caring and sacrifices for preparing me for my future. I am very much thankful from deepen my heart to my sisters (Alrabab Fergany and her husband Ahmed Tarek and Aisha Fergany) and my brother (Abdullah Fergany) for their love, prayers, and continuing support to complete this research work. I also thank all my dearest friends who support me spiritually through this work.

Last but not the least, I am thankful for all people who support me directly or indirectly through this research work.

ABBREVIATIONS

ANOVA, analysis of variance; bw, body weight; BDNF, brain derived neurotrophic factor; GCLC, glutamate-cysteine ligase, catalytic subunit; GCLM, glutamate-cysteine ligase, modifier subunit; GPX1, glutathione peroxidase 1; GPX4, glutathione peroxidase 4; GSSG; oxidized glutathione, GSTM, glutathione S transferase mu; GSTM-5, glutathione S transferase mu5; HO-1, heme oxygenase 1; IFN-γ, interferon gamma; IGF-1, insulin-like growth factor 1; IHC, immunohistochemistry; IL-18, interleukein-18; IL-1β, interleukin -1β; IL-6, interleukin-6; iNOS, inducible nitric oxide synthase; LFS, landing foot spread; MT, metallothionein 1; NA axon, noradrenergic axon; NAT, noradrenergic axon terminals;NF-kB, nuclear factor-kappa B; NQO1, NAD(P)H: quinone oxidoreductase 1; Nrf-2, nuclear factor E2-related factor 2; ROS, reactive oxygen species; S1FL, forelimb primary somatosensory cortex; S1HL, hindlimb primary somatosensory cortex; S1BF, Barrel field primary somatosensory cortex; S2, secondary somatosensory cortex;SOD-1, superoxide dismutase 1; TNF-α, tumor necrosis factor- a; TXNDL, thioredoxin L; TXNRD1, thioredoxin reductase 1; CA1, Cornu ammonis 1; CA3, Cornu ammonis 3; PAH, Poly aromatic hydrocarbon; BaP, Benzo a Pyrene.

TABLE OF CONTENTS

GENERAL ABSTRACT ---------- **1**

DEDICATION ---------- **4**

ACKNOWLEDGMENT ---------- **5**

ABBREVIATIONS ---------- **7**

TABLE OF CONTENTS ---------- **8**

1. INTRODUCTION ---------- **10**

2. LITERATURE REVIEW ---------- **12**

2.1 Electrophiles ---------- **12**

2.2 Physiochemical properties of acrylamide ---------- **12**

2.2.1 Sources of acrylamide exposure ---------- **13**

2.2.2 Mechanism of acrylamide metabolism ---------- **14**

2.2.3 Different mechanisms of acrylamide induced neurotoxicity ---------- **14**

2.2.4 IL-1β and inflammatory response ---------- **16**

2.3 Physiochemical properties of Benzo[a]pyrene ---------- **16**

2.3.1 Sources of Benzo[a]pyrene ---------- **17**

2.3.2 Different routes of exposure to Benzo[a]pyrene ---------- **17**

2.3.3 Mechanism of benzo[a]pyrene metabolism ---------- **18**

3. AIMS OF STUDY ---------- **20**

4. CHAPTER I: Deletion of *IL-1β* Exacerbates Acrylamide Induced Neurotoxicity In mice ---------- **21**

4.1 INTRODUCTION ---------- **21**

4.2 MATERIALS AND METHODS ---------- **22**

4.2.1 Chemical preparations ---------- **22**

4.2.2 Animal Husbandry and experimental design ---------- **22**

4.2.3 Landing foot spread test ---------- **24**

4.2.4 Euthanasia, tissue harvest, processing, and morphological assessment ---------- **24**

4.2.5 Cryosection of brain tissues ---------- **25**

4.2.6 Immunohistochemical examination ---------- **25**

4.2.7 Isolation of total mRNA, synthesis of cDNA and real-time quantitative polymerase chain reaction (PCR) ---------- **26**

4.2.8 Preparation of cytoplasmic and nuclear extracts for western blotting and Nrf2 activation assay ---------- **28**

4.2.9 Western blotting ---------- **29**

4.2.10 Assay for Nrf2 activation using ELISA with oligonucleotide containing ARE (Antioxidant Response Elements) consensus binding site ---------- **29**
4.2.11 Assessment of oxidative stress ---------- **29**
4.2.12 Statistical analysis ---------- **31**
4.3 RESULTS ---------- **31**
4.3.1 Body weight and brain weight ---------- **31**
4.3.2 Functional changes (Landing foot spread test) ---------- **32**
4.3.3 Morphological changes of noradrenergic axons ---------- **32**
4.3.4 Effects of acrylamide on mRNA expression ---------- **35**
4.3.5. Effects of acrylamide on HO-1, NQO-1, GSTM1 protein levels ---------- **37**
4.3.6 Effects of acrylamide on extent of Nrf2 activation ---------- **38**
4.3.7 Effects of acrylamide on total and oxidized glutathione levels ---------- **38**
4.3.8 Effects of acrylamide on malondialdehyde (MDA) ---------- **38**
4.4 DISCUSSION AND CONCLUSION ---------- **39**
5. Chapter II: Exposure to benzo[a]pyrene decreases noradrenergic and serotonergic axons in hippocampus of mouse brain---------- **42**
5.1 INTRODUCTION ---------- **42**
5.2 MATERIAL AND METHODS ---------- **42**
5.2.1 Chemicals ---------- **42**
5.2.2 Animals and Benzo[*a*]pyrene *administration* ---------- **43**
5.2.3 Functional Analysis test (Landing foot splay test) ---------- **43**
5.2.4 Sample collection ---------- **44**
5.2.5 Immunohistochemistry for noradrenergic and serotonergic axon ---------- **45**
5.2.6 RNA isolation, cDNA synthesis and quantitative polymerase chain reaction (qPCR) **46**
5.2.7 Statistical analysis ---------- **47**
***5.3* RESULTS** ---------- **48**
5.3.1 Body, brain weight and functional analysis test ---------- **48**
5.3.2 Quantification of noradrenergic and serotonergic axons ---------- **48**
5.3.3 The expression levels of selected mRNA ---------- **50**
5.4 DISCUSSION AND CONCLUSION ---------- **54**
6. REFERENCES ---------- **58**

1. INTRODUCTION

We are surrounded by numerous chemicals in all environments, which is not surprising given that the Chemical Abstracts database holds the records for 115 million small molecules. Among them, electrophiles are commonly found. The environmental electrophiles are aromatic hydrocarbon quinones formed during combustion of gasoline, crotonaldehyde in tobacco smoke, methylmercury accumulated in fish, cadmium contaminated in rice, and acrylamide in baked foods (Kumagai & Abiko, 2017). Environmental electrophilic chemicals readily react with a variety of biological nucleophiles such as GSH, cysteine, histidine, and lysine residues on proteins as well as nitrogen centers in the nucleic acids to from adducts. Among many environmental electrophiles is acrylamide and B[*a*]P.

Electrophiles have low electron-density sites that form adducts by covalently binding to nucleophilic substituents such as high electron-density DNA guanine residues and protein cysteine residues. As a result, this electrophile covalently reacts with nucleophilic moieties of DNA, resulting in the formation of DNA adducts involved in carcinoma (Berenblum, 1945; Borgen et al., 1973). These chemicals undergo biotransformation, yielding electro- philic metabolites that covalently bind to the abundant small nucleophile glutathione (GSH), leading to the GSH adducts associated with detoxification of these chemicals (Mitchell et al., 1973).

Consumers can be directly exposed to ACR *via* the oral intake of high-carbohydrate foods, such as potato chips, baked cereals, and bread (Pennisi et al., 2013). High-temperature cooking (mainly roasting, baking, and frying), such as heating potatoes (or carbohydrate-rich foods above 120 °C), yields acrylamide (M.Törnqvist, 2005; Tareke et al., 2002). As a raw material used during industrial production, ACR often enters the water, soil, atmosphere, and other environmental media, damaging human health and severely affecting the nervous system (Friedman, 2003). Occupational exposure is one of the main ACR exposure pathways. As early as the 1950s, it was reported that several workers exposed to ACR showed symptoms of poisoning, such as weakness, numbness, leg weakness, and unsteady gait (Pennisi et al., 2013). ACR exposure can occur *via* drinking water, especially when public drinking water sources are treated using polyacrylamide as a flocculant (Backe et al., 2014), leading to high ACR concentrations in tap water. ACR toxic have two pathway, Briefly, an enzymatic reaction occurs when catalyzed by the cytochrome P450 enzyme system, CYP2E1, converting ACR into glycidamide (GA) (Rifai & Saleh, 2020). Studies have found that GA can combine with purine bases on deoxyribonucleic acid (DNA) molecules to form DNA adducts, inhibit the release of neurotransmitters, cause nerve terminal degeneration, damage nerve structures, and display distinct cumulative effects. Chronic ACR poisoning can cause selective peripheral and central nerve fiber

degeneration, which initially occurs at the ends of long and large nerve fibers, followed by progressive, continuous proximal axon degeneration (Spencer & Schaumburg, 1975). Further studies show that ACR affects the levels of actin, motor proteins, and other neuronal proteins, resulting in an insufficient supply of adenosine triphosphate, impairing axonal transport functionality (An et al., 2016).

Benzo[*a*]pyrene (B[*a*]P) is one of the representatives of polyaromatic hydrocarbons (PAHs). Benzopyrene itself is inactive, but undergoes metabolic activation mediated by microsomal enzymes, forming its dihydrodiol epoxide that is unstable and rapidly converted into an electrophilic metabolite (Berenblum, 1945; Borgen et al., 1973). B[*a*]P and other PAHs have been shown to be formed during the burning of fossil fuels, wood, and other organic materials. B[*a*]P has been detected in high levels in cigarette smoke, diesel exhaust, charcoal-based foods, as well as industrial wastes (Bostrom et al., 2002). The main sources of human B[*a*]P exposure are contaminated food and the air (Bukowska & Sicinska, 2021). An important source of exposure to B[*a*]P is tobacco smoke. B[*a*]P concentrations in the side stream of cigarette smoke. Most emissions of PAHs derive from human sources, i.e., fossil fuels pyrolysis, incomplete combustion, and burning of biomass (Dejchanchaiwong et al., 2020). B[*a*]P, which is created as a result of food preparation and processing during its baking, frying, grilling, or smoking (high tem- perature processes), is an important source of this substance for humans (Sampaio et al., 2021).

Based on the above-mentioned introduction, this thesis aims to clarify the effect of different environmental proelectrophile and or electrophile on monoaminergic axons degeneration and the role of proinflammatory cytokines IL-1beta on electrophile induced neurotoxicity in mice.

2. LITERATURE REVIEW

2.1 Electrophiles

We are surrounded by numerous chemicals in all environments, which is not surprising given that the Chemical Abstracts database holds the records for 115 million small molecules. Among them, electrophiles are commonly found such as aromatic hydrocarbon quinones formed during combustion of gasoline, crotonaldehyde in tobacco smoke, methylmercury accumulated in fish, cadmium contaminated in rice, and acrylamide in baked foods. Environmental electrophilic chemicals readily react with a variety of biological nucleophiles such as GSH, cysteine, histidine, and lysine residues on proteins as well as nitrogen centers in the nucleic acids to from adducts (Kumagai & Abiko, 2017).

Electrophiles have low electron-density sites that form adducts by covalently binding to nucleophilic substituents such as high electron-density DNA guanine residues and protein cysteine residues. As a result, this electrophile covalently reacts with nucleophilic moieties of DNA, resulting in the formation of DNA adducts involved in carcinoma (Berenblum, 1945; Borgen et al., 1973). These chemicals undergo biotransformation, yielding electrophilic metabolites that covalently bind to the abundant small nucleophile glutathione (GSH), leading to the GSH adducts associated with detoxification of these chemicals (Mitchell et al., 1973). However, overdoses of the chemicals cause substanial depletion of GSH in the liver.

Exposure to such environmental electrophiles at lower levels can be tolerated because of detoxification systems; most electrophiles can be detoxified and then excreted into extracellular space by phase-II xenobiotic metabolizing enzymes and phase-III transporters. However, at higher levels that exceed the capacity of the detoxification system, electrophiles can disrupt redox signaling and cause cell damage (Kumagai & Abiko, 2017).

2.2. Physiochemical properties of acrylamide

Acrylamide is an odorless and colorless crystalline solid at room temperature. Its molecular formula is CH_2=CH–CO–NH_2 and molecular weight is 71.08. AA boiling point is 125 °C (25 mm Hg), and melting epoint is at 84.5 °C, and density is 1.27 g/ml (25 °C) (Hawley GG, 1997).

2.2.1 Sources of acrylamide exposure

2.2.1.1 Food borne exposure

Consumers can be directly exposed to ACR *via* the oral intake of high-carbohydrate foods, such as potato chips, baked cereals, and bread (Pennisi et al., 2013). High-temperature cooking (mainly roasting, baking, and frying), such as heating potatoes (or carbohydrate-rich foods above 120 °C), yields acrylamide (M.Törnqvist, 2005; Tareke et al., 2002). This process occurs via the Maillard reaction (Mottram et al., 2002). Multiple factors influence the amount of acrylamide in food, including the temperature and duration of cooking, level of moisture in the food product, and amount of reducing sugar and asparagine in fresh foods (Elmore et al., 2005; Ishihara et al., 2005). Plant food products, e.g., potatoes and cereals, contain the uppermost quantities of acrylamide because of the natural presence of glucose, fructose, or asparagine. However, meat food products include diminutive or no acrylamide owing to the absence of these ingredients (Lineback et al., 2012).

As early as 2010, the JECFA presented data regarding the ACR detected in 12,582 food samples from 31 countries, which included fried potatoes, bread, biscuits, coffee, and other food products. The results indicated the presence of ACR in almost all the analyzed food samples, with the highest levels in fried potato products and coffee (WHO, 2011). In 2011, the JECFA evaluated the dietary intake of ACR in eight representative countries. The findings showed that the average daily intake of the general population was about 1 μg/kg b.w., with the highest consumption at about 4 μg/kg b.w. (Viswanath, 2012).

2.2.1.2 Occupational exposure

As a raw material used during industrial production, ACR often enters the water, soil, atmosphere, and other environmental media, damaging human health and severely affecting the nervous system (Friedman, 2003). Those at risk for exposure to acrylamide include workers of construction manufacturing, coal mine plants, flocculator industries, acrylamide production plants, or tunnel construction. Acrylamide can be absorbed through the skin, respiratory system, or digestive system (Exon, 2006) during the process of polarization or treatment of contaminated aqueous liquid (Pennisi et al., 2013). Occupational exposure is one of the main ACR exposure pathways. As early as the 1950s, it was reported that several workers exposed to ACR showed symptoms of poisoning, such as weakness, numbness, leg weakness, and unsteady gait (Pennisi et al., 2013).

2.2.1.3 Environmental exposure

ACR exposure can occur *via* drinking water, especially when public drinking water sources are treated using polyacrylamide as a flocculant (Backe et al., 2014), leading to high ACR concentrations in tap water. In the United Kingdom, ACR was found in tap water in an area where polyacrylamide was used for water treatment (Brown L, 1982; WHO, 2011). Moreover, residual ACR is present in cosmetics (1 μg/kg b.w./day) while exposure can also occur *via* direct skin contact and alimentary contact (LuX, 2014; Smith et al., 1997), packaging materials (0.5- 8.8 mg/kg) exposure dose as ACR is widely used as a papermaking additive in many paper packages. Cigarettes also contain substantial amount of ACR, Zhang et al. examined 51 local volunteers and further correlated the exposure model with the daily intake of ACR and he found that the expected exposure dose for non-smokers 1.08 ± 0.51 μg/kg b.w./day, and smokers 4.18 ± 1.13 μg/kg b.w./day (Zhang et al., 2018)

2.2.2 Mechanism of acrylamide metabolism

ACR is small hydrophilic substance that is absorbed via the gastrointestinal tract and diffuse passively to entire human and animal body, in addition, ACR can pass the blood brain barrier and develop neurotoxicity (Koszucka et al., 2020). The ACR toxic have two pathway, (1) Briefly, an enzymatic reaction occurs when catalyzed by the cytochrome P450 enzyme system, CYP2E1, converting ACR into glycidamide (GA) (Rifai & Saleh, 2020). Studies have found that GA can combine with purine bases on deoxyribonucleic acid (DNA) molecules to form DNA adducts, inhibit the release of neurotransmitters, cause nerve terminal degeneration, damage nerve structures, and display distinct cumulative effects. In addition, the ability of GA to form Hb and DNA adducts is more significant than ACR. Therefore, it is believed that this pathway is the main route of ACR-induced neurotoxicity (Li et al., 2016; Mucci & Wilson, 2008). (2) ACR undergoes biotransformation and is catalyzed by glutathione S-transferase in the liver, combining with glutathione to generate N-acetyl-S-cysteine. It is further degraded into mercapturic ACR acids, which are excreted in the urine. This pathway is mainly responsible for ACR detoxification (Kirman et al., 2003).

2.2.3 Different mechanisms of acrylamide induced neurotoxicity

2.2.3.1 Axonal degeneration

Acrylamide can change the β-actin, β-tubulin, and other cytoskeletal proteins, destroying the neuron structures to cause neurotoxicity. Subsequent morphological, electrophysiological, and electrochemical research shows that nerve endings represent the primary target of ACR toxicity (Von

Burg et al., 1981). Chronic ACR poisoning can cause selective peripheral and central nerve fiber degeneration, which initially occurs at the ends of long and large nerve fibers, followed by progressive, continuous proximal axon degeneration (Spencer & Schaumburg, 1975). Further studies show that ACR affects the levels of actin, motor proteins, and other neuronal proteins, resulting in an insufficient supply of adenosine triphosphate, impairing axonal transport functionality (An et al., 2016). ACR, as an electrophilic reagent, can quickly attack the sulfhydryl group on proteins and react with molecular DNA while adduct formation may be a reason for its neurotoxicity (LoPachin et al., 2006). ACR can also attack protein sites containing thiols, interfere with the presynaptic nitric oxide (NO) signaling pathway, damage presynaptic nerve endings, disturb nerve signal transmission, and produce neurotoxicity (Mohr et al., 1994).

2.2.3.2 Inflammatory related pathway

The primary manifestation of immune inflammation involves inflammatory factor secretion, such as tumor necrosis factor- α (TNF-α), interleukin-1β (IL-1β), interleukin-6 (IL-6), and interleukin-18 (IL-18) (Tschopp & Schroder, 2010). Previous research by Zhao et al. found increased TNF-α, IL-6, and IL-1β levels in the primary microglia during the later stage of ACR exposure, further confirming the involvement of the immune-inflammatory response in ACR-induced neurotoxicity (Zhao et al., 2017). Recent studies have shown that the NLRP3 inflammasome level was up-regulated in the hippocampi of rats after oral ACR administration, further increasing the expression levels of pro-inflammatory cytokines, IL-1β, IL-6, and IL-18 (C. Zong et al., 2019). Liu and his colleagues reported that inflammatory factors were released *via* the microglial activation facilitated by persistent ACR exposure. NLRP3 inflammasome activation increased the level of IL-1β, raising the levels of other inflammatory factors directly responsible for neuronal injury in the cerebrums of rats (Y. Liu et al., 2020).

2.2.3.3 Oxidative stress

Recent studies have shown that oxidative stress may be involved in the occurrence and development of neurodegenerative and chronic diseases (such as stroke, diabetes, Parkinson's, Alzheimer's, and other diseases (Patil et al., 2014). The brain is more vulnerable to oxidative stress than other organs (da Silva et al., 2014; Foyet et al., 2017), and most neurocyte components can be oxidized and damaged (Chen & Zhong, 2014). ACR-induced neurotoxicity typically manifests as intracellular glutathione depletion (Kopanska et al., 2015), indicating that oxidative stress may play a significant role in ACR neurotoxicity. In recent years, some studies have demonstrated that ACR induced oxidative stress. ACR affect the cellular redox chain and it can generate reactive oxygen species (ROS). AA is oxidized

to glycidamide and then conjugate with GSH. ACR and its metabolite, glycidamide, capable to interact with nucleophiles group in cells (such as –SH, –NH2 or –OH). ACR reacts with GSH by helping of glutathione s teransferase. With increase of AA concentration, GST and SOD activity is increased and the GSH count is depleted (Chen et al., 2014; Yousef & El-Demerdash, 2006)

2.2.4 *IL-1β* and inflammatory response

Acute inflammation is a self-limiting, complex biological response mounted to combat pathogen invasion, to protect against tissue damage, and to promote tissue repair should it occur. However, unabated inflammation can be deleterious and contribute to injury and pathology. Interleukin-1β (IL-1β), a prototypical "pro-inflammatory" cytokine, is essential to cellular defense and tissue repair in nearly all tissues. With respect to brain, however, studies suggest that IL-1β has pleiotrophic effects. It acts as a neuromodulator in the healthy central nervous system (CNS), has been implicated in the pathogenic processes associated with a number of CNS maladies, but may also provide protection to the injured CNS (Hewett et al., 2012). The triad of neurons, astrocytes, and microglia is crucial to brain function. Astrocytes perform a neurotrophic role (Sofroniew & Vinters, 2010) and microglia represent the resident immune cells of the CNS (Czeh et al., 2011; Streit & Xue, 2009). Microglia activation is essential for immune surveillance protection, but excessive activation might result in the uncontrolled release of proinflammatory cytokines (Block et al., 2007). They rapidly become activated in response to injury or infection and release neurotoxic signals including reactive oxygen species (ROS) and pro-inflammatory mediators such the cytokines *IL-1*, *TNF*-α, and *IL-6* (Li et al., 2014; Sloan & Barres, 2014). Furthermore, glial cells play a crucial role in the onset and development of neurotoxicity and brain disorders (Dheen et al., 2007). CNS glia produce a substantial amount of interleukin-1 (*IL-1β*) which is a cytokine that promotes inflammation, when there is damage, stress, or illness. In the brain, *IL-1β* has a wide range of functional effects. This cytokine induces the synthesis of additional cytokines and growth factors in astrocytes and microglia, ultimately boosting inflammatory activity in the brain (Benveniste, 1992; Merrill & Benveniste, 1996).

2.3. Physiochemical properties of Benzo[*a*]pyrene

Benzo[*a*]pyrene (B[*a*]P) is one of the representatives of aromatic hydrocarbons. Having five benzene rings, B[*a*]P belongs to a group of polycyclic aromatic hydrocarbons (PAHs). A single molecule of benzene is liquid, while benzopyrene is solid. PAHs containing two or more fused benzene rings form stable molecule structures of a high hydrophobic nature (Bezza & Chirwa, 2017). Benzopyrene itself is inactive, but undergoes metabolic activation mediated by microsomal enzymes,

forming its dihydrodiol epoxide that is unstable and rapidly converted into an electrophilic metabolite (Berenblum, 1945; Borgen et al., 1973).

2.3.1 Sources of Benzo[*a*]pyrene

B[*a*]P and other PAHs have been shown to be formed during the burning of fossil fuels, wood, and other organic materials. B[*a*]P has been detected in high levels in cigarette smoke, diesel exhaust, charcoal-based foods, as well as industrial wastes (Bostrom et al., 2002). In mammals, B[*a*]P is readily absorbed after inhalation, oral administration, and through the skin (Knafla et al., 2006). The main sources of human B[*a*]P exposure are contaminated food and the air (Bukowska & Sicinska, 2021). An important source of exposure to B[*a*]P is tobacco smoke. B[*a*]P concentrations in the side stream of cigarette smoke was shown to be in the range of 52 to 95 ng/cigarette—over three times higher than in main stream smokers (IARC et al., 2010).

2.3.2 Different routes of exposure to Benzo[*a*]pyrene

Occupational exposure to PAHs, including B[*a*]P, occurs mainly through inhalation and dermal contact. The highest mean level of PAHs has been determined in aluminum production (Söderberg process) with concentrations up to 100 μg/m^3. Average levels of PAHs are detected in roof coverings and pavements (e.g., 10–20 μg/m^3), and the lowest (i.e., 1 μg/m or below) have been noted in coal liquefaction, coal-tar distillation, wood impregnation, chimneys, and power plants (IARC et al., 2010).

2.3.2.1 Air exposure

Polyaromatic hydrocarbons (PAHs), including B[*a*]P, are significant components of air pollution. Most emissions of PAHs derive from human sources, i.e., fossil fuels pyrolysis, incomplete combustion, and burning of biomass (Dejchanchaiwong et al., 2020). The highest B[*a*]P levels, reaching several dozens of nanograms per cubic meter, were found in road tunnels and in big cities, which intensively utilize coal and other fuels to heat houses (Europe.2020.; Report et al., 2021). Huge concentrations of PAHs, including B[*a*]P, are often detected in the indoor air of workplaces. Sen and his colleagues (Sen et al., 2018) assessed the exposure of iron foundry workers (Shimoga, India) to PAHs, including B[*a*]P. They detected mean concentrations of total PAHs, which were from 23.48 μg/m^3 at the melting section to 82.64 μg/m^3 at the molding section, while mean and maximum B[*a*]P levels were determined to be as high as 7.20 ± 1.11 μg/m^3 and 45.37 μg/m^3, respectively. High mean concentrations of B[*a*]P, at

levels of 14 μg/m^3 and 3.3 μg/m^3, were also determined in the indoor air of aluminum manufacturing factories and in coke oven facilities, respectively (Brandt & Watson, 2003; Ny et al., 1993).

2.3.2.2 Contaminated food

Consumption of food contaminated with B[*a*]P, which is created as a result of food preparation and processing during its baking, frying, grilling, or smoking (high temperature processes), is an important source of this substance for humans. (Sampaio et al., 2021), such as olive oil (2.19 ± 0.2 ppb), Alwana olive oil (31.3 ± 0.3 ppb) (Gharby et al., 2018), milk (0.06–2.09 μg/kg), and meat/fish-based baby foods (0.00–1.66 μg/kg) (Santonicola et al., 2017). B[*a*]P has also been determined in traditionally smoked goat cheeses, such as Wallahian-style cheese (0.85 ± 0.255 μg/kg) or smoked "Ritta" (17.0 ± 5.10 μg/kg) (Migdal et al., 2022), charcoal-grilled chicken with and without marinating at 270 °C (1.19 ± 0.31 μg/kg; 2.22 ± 0.13 μg/kg) (Wang et al., 2019), oysters (1.26 ± 1.22 μg/kg), mussels (0.24 ± 0.18 μg/kg), fresh shellfish (0.31 ± 0.42 μg/kg) (Bogdanovic et al., 2019), Iranian bread samples (mean 0.1 μg/kg) (Kamalabadi et al., 2020).

2.3.2.3 Soil contamination

Li and his colleagues (Li et al., 2020) showed that the spatial distribution of PAHs and B[*a*]P produced by industry impact the surrounding quality of soil. They pointed to following sources: combustion of coal (40.77%), exhausts from vehicles (32.94%), combustion of biomass (14.89%), and cooking (11.40%). Coal combustion and cooking were the prevalent sources (52.17%) of PAHs, as well as carcinogenic risk (46.48%) assessed by B[*a*]P toxic equivalent level in soil. The authors concluded that coal combustion mainly contributed to PAHs contamination and health risk in Taiyuan soil.

2.3.3 Mechanism of Benzo[*a*]pyrene metabolism

The metabolism of B[*a*]P involves several phases, as it also is in the case of many other hydrophobic xenobiotics (Figure 3). The first phase of biotransformation of PAHs, including B[*a*]P, involves the activity of cytochrome P450 (CYP1 family) and of microsomal epoxide hydrolase. During the first phase, PAHs are transformed to some phenols (hydroxy derivatives), phenol diols, dihy- drodiols, quinones, and reactive-diol-epoxides enantiomers. During PAHs transformation, ROS are also produced as by-products of these reactions.

Several enzymes acting within cytochrome P450, including CYP1A1, CYP1A2, and CYP1B1, have been shown to be implicated in B[*a*]P oxidation, while CYP1A1 is considered to be the most active in mammals (Barnes et al., 2018; Chung et al., 2007). B[*a*]P epoxidation by P450 at the 7,8 positions has been found to be one of the most dangerous reactions, which leads to the formation of B[*a*]P toxic metabolites. Interestingly, B[*a*]P oxidation at the 4 and 5 positions leads to the cre- ation of an inactive metabolite, which is eliminated from the organism (Bukowska, 2015). As mentioned above, CYP1A1 can convert B[*a*]P to B[*a*]P-7,8-epoxide, which (in the presence of epoxide hydrolase) is transformed to (+/−)-B[*a*]P-trans-7,8-dihydrodiol (DHD). B[*a*]P-7,8-DHD is a substrate for the reaction of the second CYP-dependent oxidation, which forms the final car- cinogenic metabolite—7β,8α-dihydroxy-9α,10α-epoxy-7,8,9,10-tetrahydrobenzo[*a*]pyrene (BPDE). It has been shown that in the cell nucleus, diol-epoxides can bind covalently to DNA, creating deoxyguanosine-DNA adducts that may lead to erroneous replication and mutagenesis (Barnes et al., 2018; Bukowska, 2015). Metabolism of B[*a*]P may therefore lead to the produc tion of electrophilic metabolites exhibiting a carcinogenic potential.

3. AIMS OF STUDY

The aim of this dissertation is to investigate the effect of different environmental pro-electrophile and or electrophile on noradrenergic axons degeneration and the role of proinflammatory cytokines *IL-1β* on electrophile induced neurotoxicity in mice.

More specifically the studies for this dissertation are designated as follow:

1. Deletion of *IL-1β* exacerbates acrylamide induced neurotoxicity in mice
2. Exposure to benzo[a]pyrene decreases noradrenergic and serotonergic axons in hippocampus of mouse brain

4. Chapter I: Deletion of *IL-1β* Exacerbates Acrylamide Induced Neurotoxicity In mice

4.1 INTRODUCTION

Acrylamide (C_3H_5NO) is a white, odorless, and water-soluble substance (Bin-Jumah et al., 2021), and an environmental electrophile commonly used in industry (Ruenz et al., 2016). Monomer acrylamide is used in the production of polymer compounds necessary for the manufacturing of plastic sheets, adhesive tapes, colors, and food packaging. Recent studies have also indicated that various cooking practices, such as roasting, baking and frying, result in the production of significant amounts of acrylamide through Maillard reaction of reducing sugars and amino acids (Tareke et al., 2000, 2002). In addition to fried/baked potatoes, coffee and bakery products also contain substantial amounts of acrylamide (Bin-Jumah et al., 2021). Acrylamide is also used in water sanitation and production of flocculators, grouts, and press fabrics. The widespread use of acrylamide in industries translates into occupational exposure with potential negative health effects (Pennisi et al., 2013).

In humans and experimental animals, acrylamide is known to cause various neuropathies and encephalopathies (Erkekoglu & Baydar, 2010; Spencer & Schaumburg, 1974). Previous reports described several cases of acrylamide exposure who presented with various neurological features ranging from numbness, leg weakness to unsteady movements. Based on these features, bioscientists and toxicologists focused on the issue of acrylamide neurotoxicity, especially acute occupational acrylamide intoxication in the construction, coal mining, flocculator manufacture, and tunnel building industries (Pennisi et al., 2013). These studies and more recent evidence from animal experiments suggest that neuroinflammation is potentially the underlying mechanism of acrylamide-induced neurotoxicity (Ekuban et al., 2021; Zong et al., 2019).

The triad of neurons, astrocytes, and microglia is crucial to brain function. Glial cells, including astrocytes and microglia, play a critical role in the central nervous system (CNS), which includes neurotrophic support, transporter regulation, pathogen clearance, promotion of neuronal development, and immune response modulation (Anderson & Swanson, 2000; Streit et al., 1988). Glial cells are rapidly activated in response to injury or infection to release neurotoxic signals, such as reactive oxygen species (ROS) and pro-inflammatory mediators (e.g., IL-1, TNF-α, and IL-6 cytokines) (Li et al., 2014; Sloan & Barres, 2014).

CNS glia produce substantial amounts of inflammation-promoting interleukin-1beta (IL-1β), following tissue damage, stress, or illness. In the brain, IL-1β has a wide range of functions; it induces the synthesis of additional cytokines and growth factors by astrocytes and microglia, ultimately

boosting brain inflammatory activity (Benveniste, 1992; Merrill & Benveniste, 1996). Our previous study found that acrylamide-induced neurotoxicity in the cerebral cortex of rats and BV-2 microglia cell line was associated with microglia activation and upregulation of pro-inflammatory cytokine genes (*IL-1β* and *IL-18*) (Zong et al., 2019). We also demonstrated that microglia activation and overexpression of pro-inflammatory cytokine genes (*IL-1β, iNOS, TNF-α*) accompanied greater acrylamide-induced sensorimotor impairment and degradation of noradrenergic and serotonergic axons in the prefrontal cortex of nuclear factor erythroid 2-related factor 2 (*Nrf2*)-null mice, compared to wild-type mice (Ekuban et al., 2021).

Nrf2 is a transcription factor involved in the process of oxidative stress. Once activated, Nrf2 is transferred to the nucleus, where it activates the transcription of downstream antioxidant protective genes. Nrf2 provides neuroprotection through enhancement and/or suppression of the expression of pro-inflammatory cytokines (Davuljigari et al., 2021; Ekuban et al., 2021; Kobayashi et al., 2016). Cultures of primary microglia released pro-inflammatory mediators, including *IL-1β, IL-6, TNF-α* and *G-CSF*, at 24 and 96 h after exposure to acrylamide (Zhao et al., 2017). Furthermore, rats exposed to acrylamide showed upregulation of *NF-κB, IFN-γ, IL-1β,* and *TNF-α* mRNAs in the liver and brain (Acaroz et al., 2018).

Based on the above background, the present study was designed to determine the role of IL-1β in acrylamide-induced neurotoxicity.

4.2 MATERIALS AND METHODS

4.2.1 Chemical preparations

Acrylamide (lot #A9099, purity >99%) was purchased from Sigma Aldrich (St. Louis, MO). Acrylamide was freshly prepared at the beginning of each week by dissolving in a G-10 ion exchange cartridge (Organo Co., Tokyo, Japan) filtered drinking water, stored at 4 °C degrees Celsius and administered by oral gavage every day in autoclaved tube.

4.2.2 Animal husbandry and experimental design

Ten-week-old male mice were used in the present study 60 male specific-pathogen free C57BL/6msSlc mice were purchased from (SLC Japan, Inc. (Tokyo) at 9-weeks of age and allowed to acclimatize for one week before the start of study. The IL-1 β KO mice were backcrossed C57BL/6msSlc having a congenicity of > 99.998 by (SLC Japan), At 6–8 weeks of age, the DNA was extracted from ear samples of each mouse and analyzed by polymerase chain reaction (PCR) to confirm its genotype using primers (Lac Z GAGGTGCTGTTTCTGGTCTTCACC, IL-1β common

CACATATCCAGCACTCTGCTTTCAG, *IL-1β* WT GGTCAGTGTGTGGGTTGCCTT). The PCR was conducted by a three-step cycle under conditions of 96 °C for 2 min followed by 35 cycles of 96°C for 20s, 59°C for 30s and 72°C for 45s.The amplified DNA samples were then run on a 2% agarose gel electrophoresis and visualized by a CCD camera (Fusion Solo S, Vilber Lourmat, Collegien, France). *IL-1β* KO mice (-/-) showed one band which confirm that all the mice were homozygous recessive. As the control, 30 specific pathogen-free age matched male C57BL/6msSlc wild type mice were purchased from SLC Japan, Inc. (Tokyo, Japan) and acclimatized to the new environment for one week before the start of treatment or toxicity studies.

All Mice were initially housed in separate cages of four, six each respectively and had access to filtered drinking water and normal chow diet (Charles River Formular-1; 5LR1) ad libitum. They were housed in a controlled environment of temperature (23–25°C), humidity (57–60%) and light (lights on at 0800 h and off at 2000 h). After the first week of acclimatization the mouse was weighed and then assigned at random to one of six groups, each consisting of 10 mice, which were exposed to acrylamide (0, 12.5 or 25 mg/kg). Groups 1 to 3 (Wild type mice) and group 4-6 (*IL-1 β* KO mice) were exposed to acrylamide. Acrylamide was dissolved in G-10 ion exchange cartridge (Organo Co., Tokyo, Japan) filtered drinking water and administered using oral gavage. Mice of each group (n=4, n=6 each) were housed in four and six per cage for morphology and biochemical analysis respectively and treated with the compounds every day of the week for four weeks. In the present study, 25 mg/kg was used as the highest exposure level for acrylamide based on the findings of previous studies in rat using 20 mg/kg body weight (Zong et al., 2019; C. Zong et al., 2019)

The protocol and experimental design of the present study were approved by the animal experiment committee of the Tokyo University of Science (Experiment approval Number Y 21016) and strictly followed the guidelines of Tokyo University of Science on animal experiments in accordance with the Japanese act on welfare and management of animals.

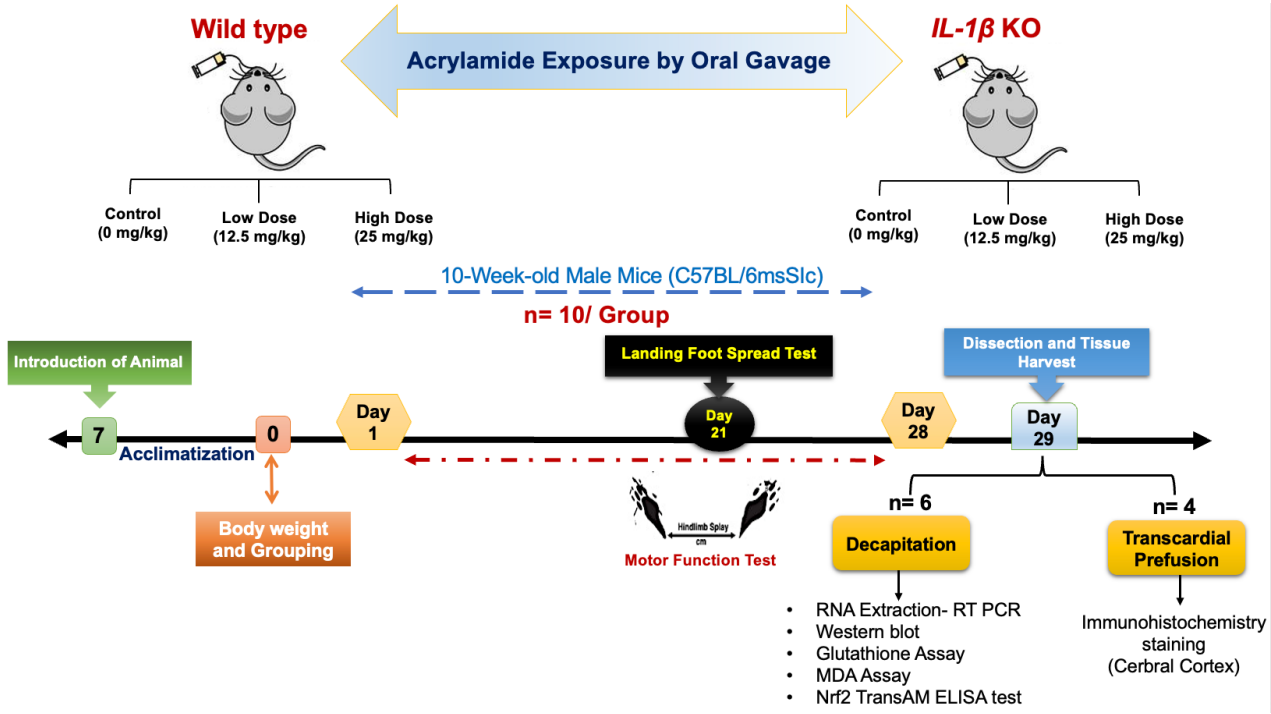

Figure 1: Schematic illustration of the experimental design. Acrylamide is used with different concentration (0, 12.5, 25 mg/kg B.W), given by oral gavage 7days/week for 28 days for both wild type and IL-1B KO mice. The mice subjected to functional test (Landing foot spread test) after 21 days of exposure. After 4 weeks of exposure, tissue harvest is done to assess biochemical changes and morphological changes using immunohistochemical staining of NA axons.

4.2.3 Landing foot spread test

The landing foot spread test was carried out in accordance with the United States Environmental Protection Agency's (USEPA) recommended protocol for functional observatory battery testing for the effects of drugs and other chemicals on the nervous system, as previously described **(Edwards & Parker, 1977b; Ekuban et al., 2021; Gilbert & Maurissen, 1982)**.

Briefly, after applying a dye ink to the soles of the hindlimbs, mice were dropped from a height of 15 cm. The hindlimb splay length is the distance between both sides' soles spread upon landing. The test was repeated three times, and the mean landing foot splay length was calculated each time and used as the representative value of individual mouse for statistical analysis.

4.2.4 Euthanasia, tissue harvest, processing, and morphological assessment

At 24 hours after the last exposure of acrylamide, mice were randomly selected and euthanized for morphological examinations. For morphological examination, mice (n=4/group) were deeply anesthetized with intraperitoneal injection of sodium pentobarbitone (50 mg/kg). Upon confirmation of loss of sensation, the animals were transcardially perfused through the ascending aorta with 4% paraformaldehyde in phosphate buffer (4% PFA). The perfused mice were wrapped in aluminum foil and kept on ice for a period of 1 hour to increase the penetrative effect of paraformaldehyde particularly

through the brain tissues. The brain was dissected out of the skull carefully and fixed for additional 24 hours at 4°C. After this, the brain was divided into three parts by cutting coronally at the anterior margin of the cerebellum and the optic-chiasm and then placed in a series of 10, 20 and 30% sucrose solutions over changing intervals of 24 hours each. Brain tissues (Cortex area) were then embedded in optimum cutting temperature (OCT) medium with the use of plastic Tissue Tek cryomolds (SFJ 4566, Sakura, Japan) and then stored at -80°C.

4.2.5 Cryosection of brain tissues

Brain tissues (Cortex) embedded in O.C.T. medium were serially sectioned in the coronal plane on a freezing microtome (Leica CM3050S, Leica Microsystems, Wetzlar, Germany) at 40 μm thickness from bregma Bregma –0.34 according to Paxinos and Franklin **(Paxinos & Franklin, 2004)**, which is representative of the full extent of somatosensory cortex in mice. The tissue sections were placed on positively charged slides (Matsunami MAS superfrost slides, Matsunami Glass Ind., Osaka, Japan) and allowed to air-dry at room temperature for about 1 h, after which they were stored at -80 ◦C for immunostaining.

4.2.6 Immunohistochemical examination

4.2.6.1. Noradrenergic axons staining

The frozen section in -80 °C allowed to air dry in RT for about 30 min, the air-dried sections were rinsed in Tris buffered saline (TBS; 50 mM Tris, 0.15 mM NaCl, pH 7.5-7.8) and transferred into an antigen retrieval solution containing 10 mM sodium citrate buffer (pH 8.5) that had been pre-heated to and maintained in a water bath at 80°C for 30 min. After the incubation, the sections were cooled to room temperature together with the buffer solution and washed in Tris-buffered Saline with 0.01% Tween-20 (TBST) for three times/5 min for each. Endogenous peroxidase activity was blocked for 20 minutes by incubating the sections with peroxidase blocking reagent Bloxal (Vector Laboratories, Burlingame, CA, USA). After triple washing in TBST, non-specific protein binding was blocked at 4°C overnight using protein blocking reagent [1% bovine serum albumin (BSA; Sigma Aldrich), 2.5% normal horse serum (NHS; Vector Laboratories, Burlingame, CA), 0.3M glycine (Wako) and 0.1% Tween-20 (Wako)]. This was followed by brief incubation at 37°C for 30 minutes followed by rinsing three times in TBST. Endogenous interferences of Avidin-Biotin were blocked by incubating the sections in avidin/biotin blocking reagent (Sp-2001; Vector Laboratories), as described by the manufacturer. The sections were then incubated for 2 hours at 37°C with mouse anti-noradrenaline transporter antibody (NAT; 1:1000, #ab211463, Abcam, Japan). Following incubation with the primary antibody, the sections were washed three times and then incubated for 1 hour with horse anti-mouse biotinylated secondary antibody (BA-2000; Vector Laboratories) and further washed three times in TBST. Finally, the sections were stained with the avidin-biotin peroxidase complex (Elite

ABC reagent, Vector Laboratories) and visualized by reacting with diaminobenzidine peroxidase substrate as the chromogen (ImmPACT DAB (Brown) peroxidase substrate SK-4105, Vector Laboratories), the DAB peroxidase reaction was stopped and rinsed with water, followed with three times in TBS. The sections were wiped off any liquid, allowed to air-dry and mounted with an aqueous mounting medium (VectaMount Mounting Medium, H-5501, Vector Laboratories).

4.2.6.2. Morphometric analysis of noradrenergic axons

Uncompressed photomicrographs of the stained somatosensory cortex regions were taken with a Leica FlexCam C1 digital camera-assisted microscope (BX 50, Olympus, Tokyo.), using the whole area with the vessel analysis plugin in the ImageJ software (Schneider et al., 2012). The density of noradrenergic axons was quantified in the primary somatosensory cortex (S1) of forelimb (S1FL), hindlimb (S1HL) and barrel field (S1BF) and secondary somatosensory cortex (S2) sub-regions of the somatosensory cortex at Bregma –0.34 (Paxinos & Franklin, 2004), using a 300 μm × 300 μm, modified from (Davuljigari et al., 2021) square sampling frame with the vessel analysis plugin in the ImageJ software (Schneider et al., 2012). We also determined the vascular density, which represented the ratio of the vessel area relative to the total area multiplied by 100%. These studies were conducted in 4 mice and 2 sections from each were used for analysis.

4.2.7. *Isolation of total mRNA, synthesis of cDNA and real-time quantitative polymerase chain reaction (PCR)*

Total messenger RNA (mRNA) was isolated from the cerebral cortex (n=6/ each group) using the ReliaPrep™ RNA Tissue Miniprep System (Promega, Madison, WI), according to the instructions provided by the manufacturer. The concentration of the extracted mRNA following elution with RNase-free water was measured using NanoDrop 2000 spec-trophotometer (Thermo Fisher Scientific, Waltham, MA). The quality of mRNA was determined by confirming that the A260/A280 ratio was ≥2.0 after measuring absorbance at 260 nm and 280 nm. Complementary DNA (cDNA) was then synthesized by using 4μg of the extracted total RNA with SuperScript III reverse transcriptase (Invitrogen, Carlsbad, CA) according to the instructions supplied by the manufacturer. Real-time quantitative PCR was performed by using the THUNDERBIRD® SYBR® qPCR Mix (Toyobo, Osaka) and the AriaMx Real-Time PCR System (Agilent Technologies, Santa Clara, CA). The PCR reaction component (20 μL final volume): cDNA 2 μL, forward primer (10 μM) 0.4 μL, reverse primer (10 μM) 0.4 μL, SYBR qPCR mix 10 μL, 50X ROX reference 0.04 μL and nuclease free water 7.16 μL. A three-step real-time PCR amplification reaction comprising an initial denaturation step at 95ºC for 1 min, followed by an amplification step of 40 denaturation cycles at 95ºC for 15 sec, primer

annealing at 60ºC for 30 sec, extension at 72ºC for 60 sec and reading of plate was utilized. A melting curve step from 55 to 95ºC with 0.5ºC increments for 5 sec followed by a plate read was also incorporated. A standard curve constructed using serial concentrations of diluted cDNA samples from the control group was used to quantify the relative expression level of each gene. The latter was calculated by standardization to the endogenous mRNA levels of the housekeeping gene β-actin. The mRNA expression levels of *Nrf2* and antioxidant genes: heme oxygenase 1 (*Ho-1*), NAD(P) H: quinone oxidoreductase 1 (*Nqo1*), superoxide dismutase -1 (*Sod-1*), glutathione-s-transferase mu (*Gst-m*), glutathione-s-transferase mu-5 (*Gst-m5*), thioredoxin reductase 1 (T*xnrd1*), thioredoxin reductase *L (TxnL)* and metallothionein 1 (*Mt-1*), glutathione peroxidase 1 (*Gpx1*), glutathione peroxidase 4 (*Gpx4*), glutamate-cysteine ligase, catalytic subunit (*Gclc*), and glutamate-cysteine ligase, modifier subunit (*Gclm*), as well as genes of several pro-inflammatory cytokines, including interleukin -6 *(IL-6*), interleukin-18 (*IL-18*), nuclear factor kB (*Nf-kB*), caspase-1, tumor necrosis factor alpha (*TNF-α*), inducible nitric oxide synthase (*Nos2*), and cyclooxygenase 2 (*Cox-2*) were analyzed. Primer sequences for the various genes are listed in **(Table 1).**

Table 1: Primer sequences for the various genes used in this study

Gene	Primer Sequence	Reference
Nfe2l2 (Nrf2)	F: CGAGATATACGCAGGAGAGGTAAGA R: GCTCGACAATGTTCTCCAGCTT	(Jiang et al., 2016)
Ho-1	F: CACAGATGGCGTCACTTCCGTC R: GTGAGGACCCACTGGGAGGAG	(Innamorato et al., 2010)
Nqo1	F: AGCGTTCGGTATTACGATCC R: AGTACAATCAGGGCTCTTCTCG	(Sehsah et al., 2019)
Gst-m (Gstμ)	F: CTGAAGGTGGAATACTTGGAGC R: GCCCAGGAACTGTGAGAAGA	(Shanmugam et al., 2017)
Mt-1	F: ACCTCCTGCAAGAAGAGCTG R: GCTGGGTTGGTCCGATACTA	(Kim et al., 2012)
Txndr1	F: GGGTCCTATGACTTCGACCTG R: AGTCGGTGTGACAAAATCCAAG	(Checker et al., 2012)
Gst-m5	F: AGAAACGGTACATCTGTGGGG R: GGATGGCGTTACTCTGGGTG	(Chung et al., 2013)
Sod-1	F: CAGGACCTCATTTTAATCCTCAC R: TGCCCAGGTCTCCAACAT	
Txndl	F:GGGAGCGATCCAGATTTCCAG R:CAATGGGAAGACAGGGTCCAC	
Il-6	F: CCTACCCCAATTTCCAATGCT R: TATTTTCTGACCACAGTGAGGAAT	
Cox-2	F: TTCGGGAGCACAACAGAGT R: TAACCGCTCAGGTGTTGCAC	(Innamorato et al., 2008)
NfkB	F: ATTCCGCTATGTGTGTGAAGG R: GTGACCAACTGAACGATAACC	
Casp1	F: TCCGCGGTTGAATCCTTTTCAGA R: ACCACAATTGCTGTGTGTGCGCA	(Mezzaroma et al., 2011)
Nos2	F: CCTCCTTTGCCTCTCACTCTT R: AGTATTAGACGCGTGGCATGG	
Tnf-α	F: CATCTTCTCAAAATTCGAGTGACAA R: TGGGAGTAGACAAGGTACAACCC	(Innamorato et al., 2008)
Il-18	F: TGGTTCCATGCTTTCTGGACTCCT R: TTCCTGGGCCAAGACGAAGTGATT	
Gpx1	F: AAGGAGGTGCAGGCGGCTGTGAGC G R: GCGCGGAGAAGGCATACACGGTGG	
Gpx4	F: TGTGCATCCCGCGATGATT R: CCCTGTACTTATCCAGGCAGA	
Gclc	F: AGATGATAGAACACGGGAGGAG R: TGATCCTAAAGCGATTGTTCTTC	
Gclm	F: CCTTGGAGCATTTACAGCCTTACT R: AGTTCTTTCGGGTCATTGTGAGTC	
Actb	F: TCCTTCCTGGGCATGGAG R: AGGAGGAGCAATGATCTTGATCTT	(Rojo et al., 2008)

4.2.8 *Preparation of cytoplasmic and nuclear extracts for western blotting and Nrf2 activation assay*

Cytoplasmic and nuclear extracts were prepared from the cerebral cortex tissues using NE-PER Nuclear and Cytoplasmic Extraction Reagent 78833 (Thermo Fisher Scientific Inc., Rockford, IL). The cytoplasmic and nuclear extracts were used for western blotting and Nrf2 activation assay, respectively.

4.2.9 Western blotting

The protein concentration in the cytoplasm was determined using Pierce 660nm Protein Assay Reagent (Pierce Biotechnology, Waltham, MA). The concentration-adjusted protein solutions were mixed with the sample buffer (final concentration; 62.5mM Tris-HCl, pH 6.8, 2% SDS, 10% glycerol, 0.0075% bromophenol blue, 5% β-mercaptoethanol) and boiled at 95℃ for 5 min. Each 10 μg protein sample was separated on Mini-PROTEAN TGX Gels 4-20% (Bio-Rad Laboratories Inc., Hercules, CA) and transferred onto PVDF membranes. Protein-blocking was applied using BlockPRO Blocking Buffer (BF01-1L, Visual Protein, Taipei, Taiwan) for 30-60 min. The membranes were incubated overnight at 4℃ with the primary antibody dissolved in 1% BSA/TBS-T: anti-β-actin rabbit mAb (4970S, dilution 1:5000; Cell Signaling Technology, Danvers, MA), anti-NQO1 rabbit mAb (11451-1-AP, dilution 1:5000; Proteintech Group, Inc, Rosemont, IL), anti-GSTM1 rabbit mAb (12412-1-AP, dilution 1:5000; Proteintech), anti-HO-1 rabbit mAb (ab13243, dilution 1:4000; Abcam) or IL-6 (D5W4V) XP® rabbit mAb (#12912, dilution 1:2000, Cell Signaling Technology) and then incubated with the secondary antibody; goat anti-rabbit IgG-peroxidase Ab (A0545, dilution 1:40000; Sigma-Aldrich) dissolved in 1% BSA/TBS-T at room temperature for 1hour. Protein bands were emitted with ImmunoStar Zeta (FUJIFILM Wako Pure Chemical) for NQO1, GSTM1, HO-1, IL-6 and β-actin, followed by visualization in Fusion Solo S (Vilber Lourmat, Collégien, France).

4.2.10 Assay for Nrf2 activation using ELISA *with oligonucleotide containing ARE (Antioxidant Response Element) consensus binding site*

TransAM®Nrf2 (Active Motif, Carlsbad, CA) was used to quantify Nrf2 activation using the method supplied by the manufacturer. Active Nrf2 was captured by the kit component 96-well plate with an immobilized oligonucleotide containing ARE consensus binding site (5′-GTCACAGTGACTCAGCAGAATCTG-3′). Anti-Nrf2 antibody followed by HRP-conjugated antibody and color developing was applied to the nuclear extracts, and absorbance at 450 and 655 nm was measured as the extent of Nrf2 activation. The final absorbance was calculated by subtraction of the value at 450 nm from the value at 655 nm. Twenty five μg nuclear protein per well was applied in this ELISA-based assay.

4.2.11 Assessment of oxidative stress

4.2.11.1 Glutathione assay (Quantification of total and oxidized glutathione)

Since the quantity of the cortical samples available for glutathione assay was inadequate, the cerebellum was used in this part of the study as a surrogate for the cerebral cortex. Cerebellar levels of total glutathione and oxidized glutathione were measured using glutathione assay kit #703002 (Cayman Chemical Company, Ann Arbor, MI). Frozen cerebellum was broken into powder on aluminum foil

placed on a stainless steel block pre-cooled by liquid nitrogen, and well mixed. Approximately 25 mg of frozen powdered cerebellar tissue sample was homogenized in 250µL of 50 mM 2-(N-morpholino), ethanesulphonic acid (MES) buffer containing 2 mM ethylenediaminetetraacetic acid (EDTA). The homogenate was centrifuged at 10,000× *g* for 15 min at 4ºC. The supernatant was then deproteinated with an equal volume of 0.1% metaphosphoric acid (#239275; Sigma Aldrich) and mixed by vortex. The resultant mixture was allowed to stand at room temperature for 5 min and centrifuged at 2000× *g* for 2 min. The supernatant was aliquoted and stored at –20ºC until analysis of total and oxidized glutathione. In the next step, 40 µL of the supernatant was treated with 2 µL of 4 M solution of triethanolamine (TEAM; Sigma Aldrich) and vortexed immediately. For determination of total reduced glutathione (GSH), 20 µL TEAM-treated sample was diluted 10-fold using the MES buffer. Subsequently, 50 µL of the diluted sample was added to 150 µL freshly prepared assay cocktail (mixture of cofactors, enzymes and DNTB reconstituted in MES buffer) and incubated for 25 min. Absorbance of the mixture at 405 nm was measured with a microplate reader (Gen5TM Secure, BioTek® Instruments, Inc. Charlotte, VT).

To determine the level of oxidized glutathione (GSSG), 20µL of the TEAM-treated sample was diluted 5-fold with MES buffer and 100µL of the diluted solution was derivatized with 1 µL of 2-vinylpyridine (Sigma Aldrich). The mixture was vortexed and incubated for 1 h at room temperature. Next, 50 µL of the derivatized sample was mixed with 150 µL of freshly prepared assay cocktail as explained earlier, incubated for 25 min in the dark and then the absorbance of mixture was measured at 405 nm using a microplate reader. The concentrations of GSH and GSSG were calculated using a standard plot with GSSG standard provided with the kit and expressed in mM/mg protein of GHS or GSSG.

4.2.11.2 Malondialdehyde assay

The cerebellum was also used as a surrogate for cerebral cortex in malondialdehyde (MDA) assay. Cerebellar MDA level was measured using NWLSS^{TM}, Malondialdehyde kit (NWK-MDA01, Northwest Life Science Specialties, LLC, Vancouver, WA) and the instruction provided by the manufacturer. Briefly, 25 mg of frozen powdered cerebellar tissue sample was homogenized in cold assay buffer, centrifuged at 5000x*g* for 15 min, then the supernatant was stored on ice. Next, 30 µL of the sample was diluted 5 times with the cold assay buffer, then 150µL of the diluted sample or the calibrator was mixed with 6µL of butylated hydroxytoluene (BHT) reagent, 150µL of acid reagent and 150µL of 2-thiobarbituric acid (TBA) reagent. The mixture was vortexed vigorously, then incubated at 60ºC for 60 minutes. One hour later, the mixture was centrifuged at 10000x*g* for 2-3 minutes, then transferred to a microplate and absorbance was measured at 532 with a microplate reader (Gen5TM

Secure, BioTek® Instruments, Inc. Charlotte, VT). Finally, MDA concentration was calculated using the MDA colorimetric standard curve and expressed in mM/mg protein of MDA.

4.2.12 Statistical analysis

Statistical analysis was performed using GraphPad Prism version 9.0 (GraphPad Software, La Jolla, CA) or JMP (version 14, SAS Institute, Cary, NC). Data are expressed as mean ± standard deviation (SD) or ± standard error of the mean (SEM), as indicated. Differences among groups in each genotype of wild-type and *IL-1β* KO mice were analyzed by one-way ANOVA followed by Dunnett's multiple comparison test. When ANOVA showed difference between groups, simple regression analysis with independent variable of ACR level was carried out in each genotype to test the trend with ACR exposure level and multiple regression analysis with independent variables of ACR level and genotype, which is defined by dummy variable (0: wild type and 1: *IL-1β* KO), in the full model with interaction was carried out to test the interaction between ACR level and genotype. A probability (p) of <0.05 denoted the presence of a statistically significant difference, except that p value was empirically determined for the criteria in simple regression analysis to identify genes whose expressions were ACR level-dependently changed in the transcriptome analysis

4.3 RESULTS

4.3.1 Body weight and brain weight

Dunnett's multiple comparison following ANOVA showed that acrylamide exposure at 12.5 and 25 mg /kg B.W did not affect body weight and brain weight in both wild type and *IL-1β* KO mice. **(Table 2)**.

Table 2: ANOVA test analysis of acrylamide effect and *IL-1β* deletion on the body weight and whole brain weight in wild type and *IL-1β* KO mice

Test parameters	Treatment	Concentration of Acrylamide (mg/kg body weight)		
		0	**12.5**	**25**
Body Weight (g)	**Wild Type**	24.88 ± 0.77	24.71± 1.14	24.57 ± 0.2
	***IL-1β* KO**	27.33 ± 2.26	27.18 ± 1.74	27.08 ± 1.7
Whole brain (mg)	**Wild Type**	682.8 ± 512	472.18± 20.64	451.33 ±7.05
	***IL-1β* KO**	459.2 ± 13.38	469.85 ± 36.2	447.63 ± 8.4

Abbreviation: ACR, acrylamide. Data are mean ± SD. *p < 0.05, compared with the corresponding genotype control by Dunnett's multiple comparison following ANOVA for the body weight (n = 10) and whole brain weight (n = 6).

4.3.2 Functional changes (Landing foot spread test)

Dunnett's multiple comparison following ANOVA showed that exposure to acrylamide dose-dependently increased the foot spread (hind limb splay) with a significant change at 25 mg/kg in *IL-1β* KO mice, but ANOVA did not show any difference between groups in wild-type mice. Multiple regression analysis showed significant interaction between ACR level and *IL-1β* KO genotype, suggesting different intensity of ACR-induced increase in hindlimb splay length by genotype **(Figure 2)**.

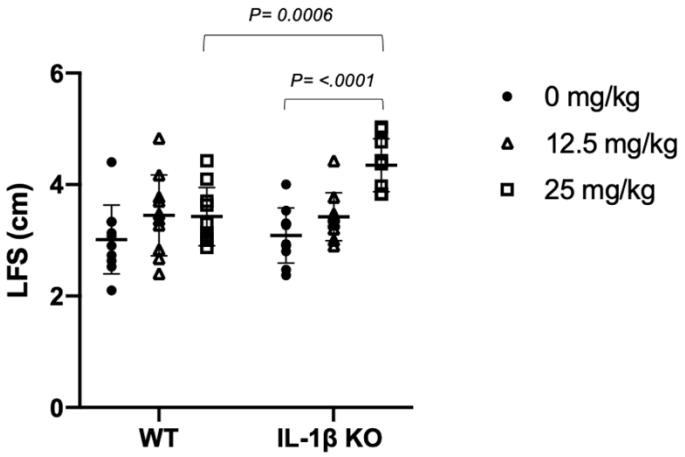

Figure 2. Functional effects of acrylamide (0, 12.5, 25 mg/kg bw) on the landing foot spread (LFS) test in wild-type and *IL-1β* KO mice. The effect was significant in *IL-1β* KO mice than wild-type mice at 25 mg/kg bw (n=10, ANOVA followed by Dunnett's multiple comparison test). Differences in the results of exposure to 25 mg/kg bw between wild-type and *IL-1β* KO mice were also examined by the Student's *t-test.* Data are mean±SD.

4.3.3 Morphological changes of noradrenergic axons

The density of noradrenergic-immunoreactive axons was quantified in the primary (S1HL, S1BF, S1FL) and secondary (S2) regions of the somatosensory cortex **(Figures 3-6)**.

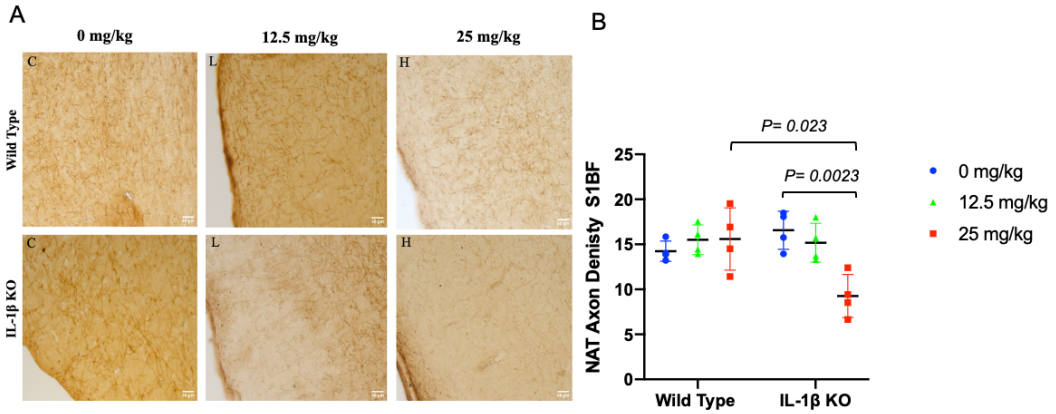

Figure 3. Representative photomicrographs (A) and density of noradrenaline transporter (NAT)-immunoreactive axons in the Barrel field primary somatosensory cortex (S1BF) following exposure to acrylamide at 0, 12.5, 25 mg/kg bw in wild-type and *IL-1ß* KO mice. Scale bars = 40 µm, n=4, each. Data are mean±SD. Statistical analyses by Student's t-test.

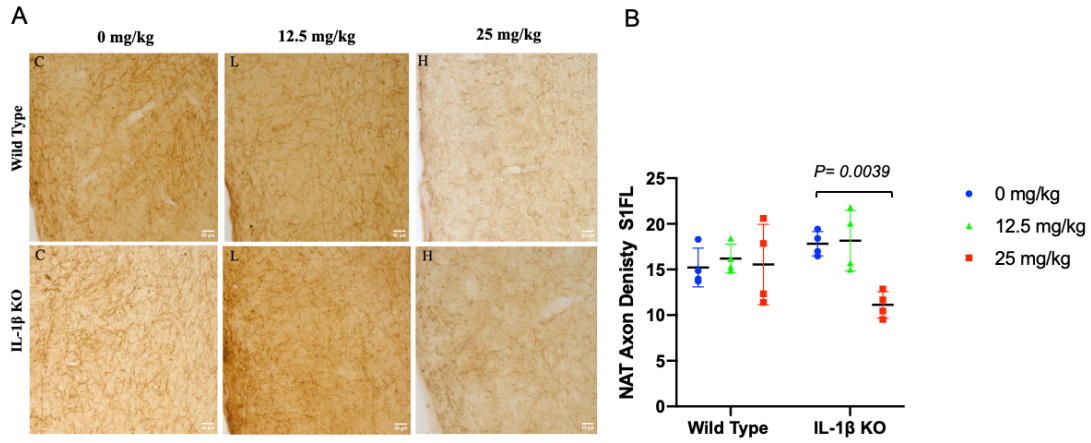

Figure 4. Representative photomicrographs (A) and density of noradrenaline transporter (NAT)-immunoreactive axons in the forelimb primary somatosensory cortex (S1FL) following exposure to acrylamide at 0, 12.5, 25 mg/kg bw in wild-type and *IL-1ß* KO mice. Scale bars=40 µm, n=4, each. Data are mean±SD. Statistical analyses by Student's t-test.

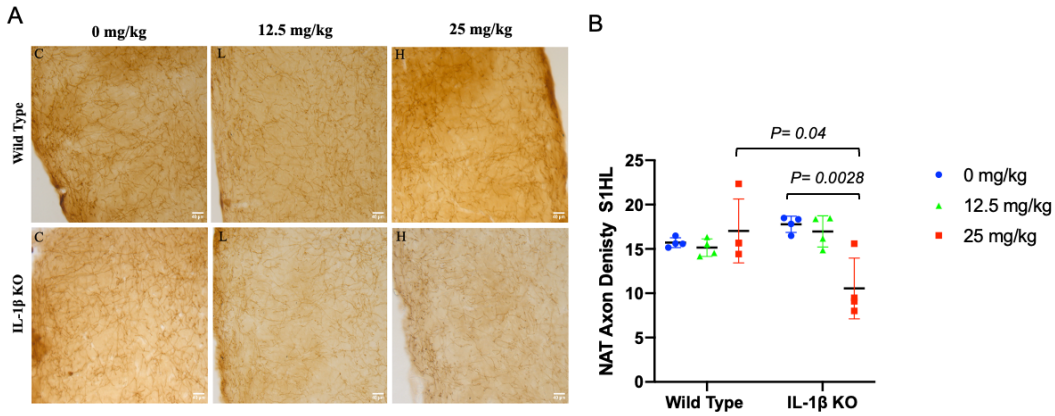

Figure 5. Representative photomicrographs (A) and density of noradrenaline transporter (NAT)-immunoreactive axons in the hindlimb primary somatosensory cortex (S1HL) following exposure to acrylamide at 0, 12.5, 25 mg/kg bw in wild-type and *IL-1β* KO mice. Scale bars = 40 µm, n=4, each. Data are mean±SD. Statistical analyses by Student's t-test.

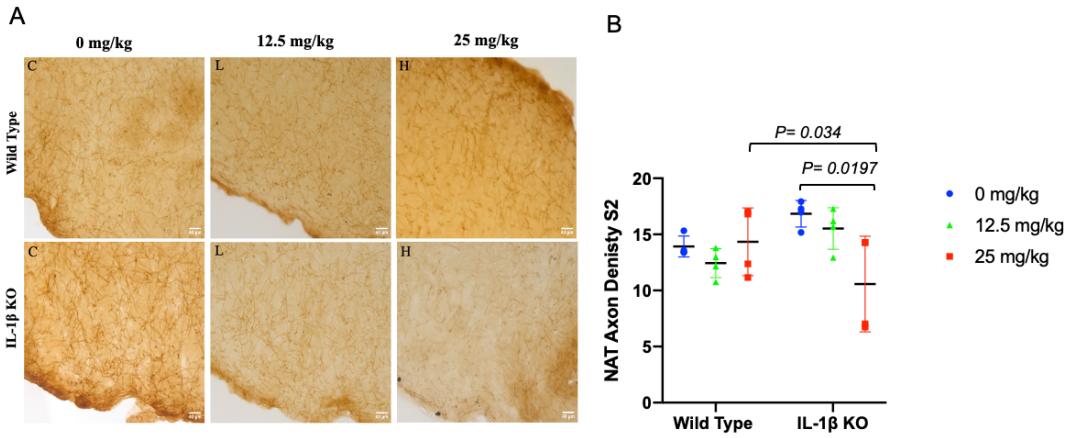

Figure 6. Representative photomicrographs (A) and density of noradrenaline transporter (NAT)-immunoreactive axons in the secondary somatosensory cortex (S2) following exposure to acrylamide at 0, 12.5, 25 mg/kg bw in wild-type and *IL-1β* KO mice. Data are mean ± SD. Statistical analyses by Student's t-test.

ANOVA followed by Dunnett's multiple comparison and simple regression analysis showed that exposure to ACR dose-dependently decreased the density of noradrenergic (NA) axons with a significant change at 12.5 or 25 mg/kg in S1BF, S1FL, S1HL and S2 of *IL-1β* KO mice. On the other hand, exposure to ACR dose-dependently decreased the density of NA axons in S1HL of wild-type mice with a significant change at 25 mg/kg but did not significantly change the density of NA axons in other investigated somatosensory cortex area **(Table 3)**.

Table 3: Results of simple regression analysis of the effect of acrylamide and multiple regression analysis of the interaction of acrylamide and IL-1*β* deletion on the landing foot spread test (LFS) (n=10/group) and the density of noradrenergic-immunoreactive axons in the primary and secondary somatosensory cortex areas (S1BF, S1FL, S1HL, S2) (n=4/group).

	Genotype	Coefficient of ACR (n=4/group) in simple regression analysis	Interaction of ACR and *IL-1β* KO in multiple regression analysis
Landing Foot Spread Test	Wild -type	-	0.034 (p=0.019)
	IL-1β KO	0.05 (p<0.0001)	
Density of NA axons in S1BF (%)	Wild-type	-	-0.34 (p=0.0013)
	IL-1β KO	-0.29 (p=0.0016)	
Density of NA axons in S1FL (%)	Wild -type	-	-0.28 (p=0.0224)
	IL-1β KO	-0.26 (p=0.0075)	
Density of NA axons in S1HL (%)	Wild -type	-	-0.34 (p=0.0019)
	IL-1β KO	-0.28 (p=0.0028)	
Density of NA axons in S2 (%)	Wild -type	-	-0.26 (p=0.0131)
	IL-1β KO	-0.25 (p=0.0099)	

Abbreviation: ACR, acrylamide; NA, Noradrenergic axon; Primary somatosensory cortices (S1BF: barrel field; S1FL: forelimb; S1HL: hindlimb). Data are mean ± SD. * $p < 0.05$, compared to the corresponding genotype control by Dunnett's multiple comparison following ANOVA for the density noradrenergic axons (n = 4). Simple regression analysis in each genotype (n = 12 per each genotype) and test for interaction in multiple regression model with dummy variable (0: wild type and 1: IL-1β knockout mice) for genotype were conducted for density of noradrenergic axons. When interaction was not significant for density of noradrenergic axons (S1FL, S1HL and S2), multiple regression analysis in a model without interaction was conducted to estimate the effect of acrylamide or *IL-1β* deletion.

4.3.4 Effects of acrylamide on mRNA expression

4.3.4.1 Nrf-2 and antioxidant genes

Exposure to acrylamide at 25 mg/kg bw significantly increased the mRNA expression levels of *Nrf-2*, heme oxygenase 1 (*Ho-1*) and NAD(P)H: quinone oxidoreductase 1(*Nqo-1*) and increased the mRNA expression level of glutathione S-transferase mu (*Gstm*), with a significant change at 12.5 mg/kg in wild-type mice (ANOVA followed by Dunnett's multiple comparison test, Figure 6A) but there was no significant interaction between acrylamide concentration and *Nrf2* deletion for the above genes. Exposure to acrylamide at 25 mg/kg bw significantly increased the expression levels of *Gpx1, Gpx4* and *Gclc* in wild-type mice, while significantly decreased the expression of *Gpx1, Gpx4* and *Gclc* in *IL-1β* KO mice (ANOVA followed by Dunnett's multiple comparison test, Figure. 7A). Multiple regression analysis showed significant interaction between acrylamide concentration and Nrf2 deletion for *Gpx1, Gpx4* and *Gclc*, suggesting significant effect of *IL-1β* deletion on the rate of acrylamide-induced change in the above genes (Supplementary Table 1). Acrylamide had no effect on the expression of other investigated antioxidant genes in both the wild-type and *IL-1β* KO mice (ANOVA, Figure 7A, 10A).

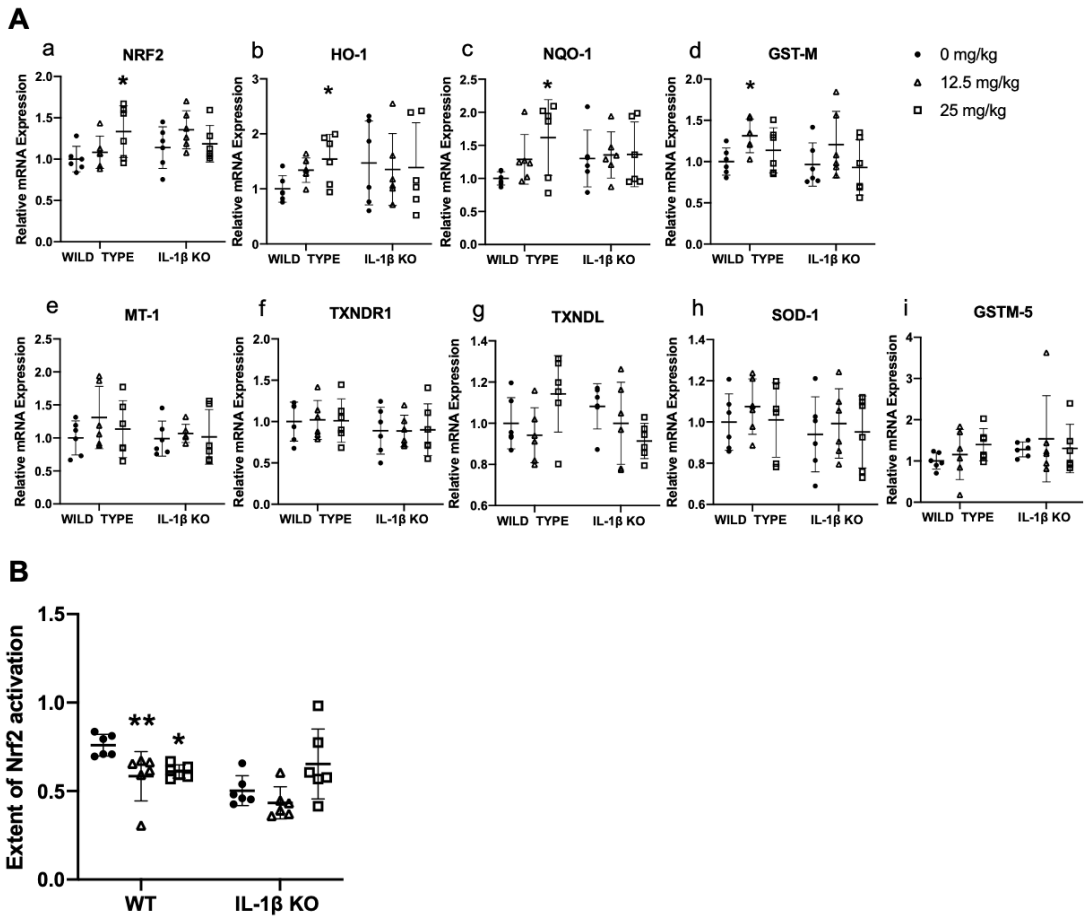

Figure 7. (A) Changes in *Nrf-2* (a), *Ho-1* (b), *Nqo*-1 (c), *Gstm* (d), *Mt-1* (e), *Txnd1* (f), *Txnl* (g), *Sod-1* (h), *Gstm-5* (i) in the cerebral cortex of wild-type and *IL-1β* KO mice exposed to acrylamide at 0, 12.5, 25 mg/kg bw for 28 days. (B) The extent of Nrf2 activation using ELISA test. Data are mean ± SD. *P< 0.05, compared to the corresponding genotype control (by Dunnett's multiple comparison following ANOVA). (n=6, each)

4.3.4.2 Pro-inflammatory cytokines

Exposure to acrylamide dose-dependently increased the mRNA expression of IL-6 with a significant change at 25mg/kg bw in wild-type mice, but no such effect was noted in IL-1β KO mice (ANOVA followed with Dunnett's multiple comparison test, Figure. 8).

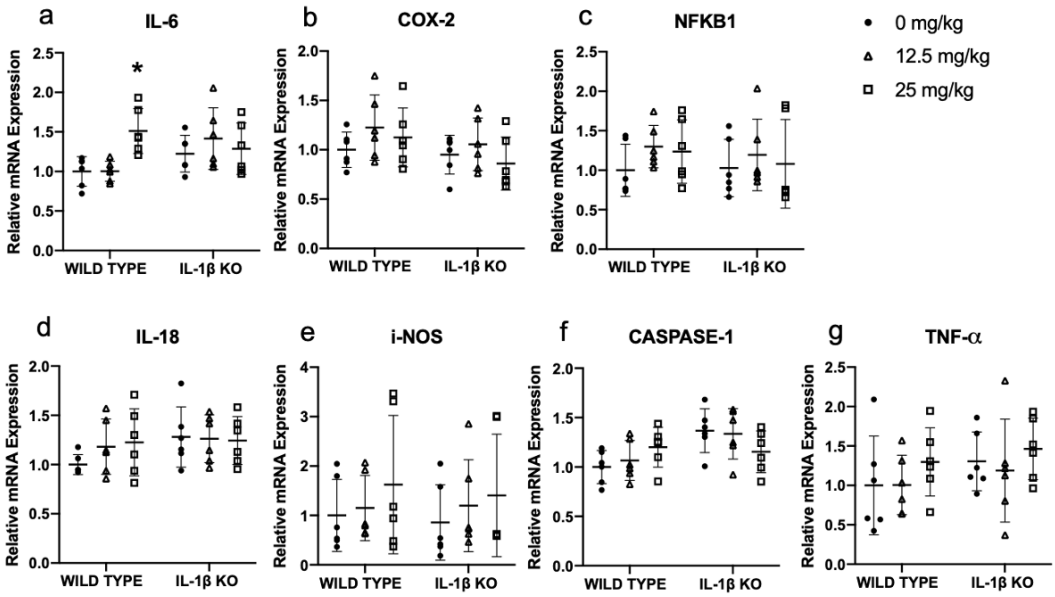

Figure 8. Changes in the mRNA expression levels of pro-inflammatory cytokines: *IL-6* (a), *Cox-2* (b), *Nfkb1* (c), *Il-18* (d), *i-Nos* (e), *Caspase*-1 (f), *Tnf-a* (g), in the cerebral cortex of wild-type and *IL-1β* KO mice exposed to acrylamide at 0, 12.5, 25 mg/kg bw for 28 days. Data are mean ± SD. *P< 0.05, compared to the corresponding genotype control (by Dunnett's multiple comparison following ANOVA).

4.3.5 Effects of acrylamide on HO-1, NQO1 and GSTM1 protein levels

The protein levels of IL-6, HO-1, NQO1 and GSTM1 were measured in wild-type and IL-1β KO mice by western blot technique. Exposure to acrylamide had no significant effect on IL-6, HO-1, NQO1 and GSTM1 protein levels in both genotypes (Figure. 9).

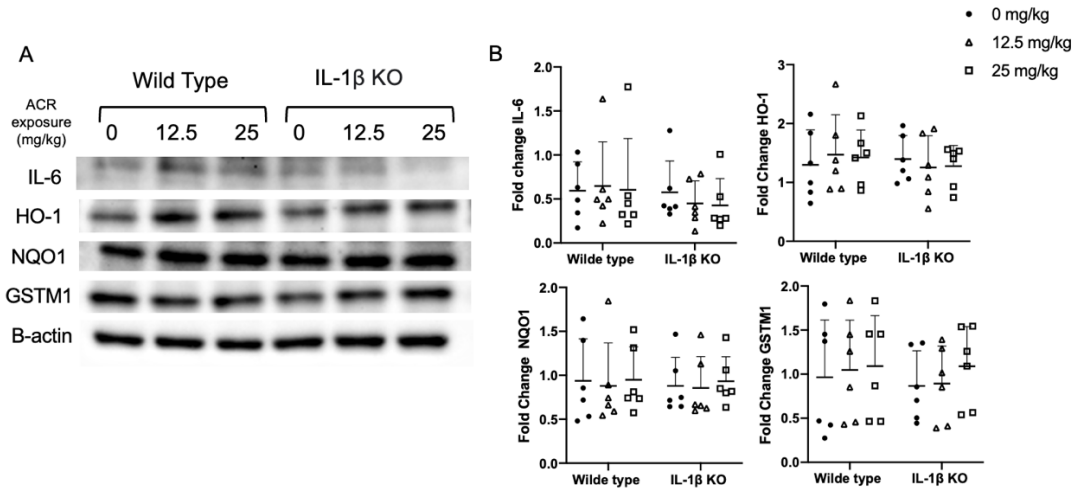

Figure 9. Changes in expression of proteins related to Nrf2-regulated antioxidative response in mice cerebral cortex. Protein expression in the cerebral cortex of control and acrylamide exposed mice as determined by western blotting. β-actin was used as a loading control. (A) Target protein were as follows: NQO1 (31kDa), GSTM1 (27kDa), HO-1 (31kDa), IL-6 (24kDa). (B) Quantification of the relative intensity of the bands, (n=6) for each group. Data are mean±SD. *p<0.05, compared with the control group of each genotype, by ANOVA followed by Dunnett's multiple comparison test

4.3.6 Effects of acrylamide on extent of Nrf2 activation

The extent of Nrf2 activation was measured by ELISA using oligonucleotide containing the ARE consensus binding site. Exposure to acrylamide dose-dependently decreased the extent of Nrf2 activation with significant changes at 12.5 and 25 mg/kg bw in the wild-type but not in IL-1β KO mice (Figure 7B).

4.3.7 Effects of acrylamide on total and oxidized glutathione levels

Exposure to acrylamide at 25 mg/kg bw significantly increased the levels of total glutathione and oxidized glutathione (GSSG) in wild-type mice but significantly decreased oxidized glutathione and the ratio of GSSG/GSH in IL-1β KO mice (ANOVA followed by Dunnett's multiple comparison test, Figure 10B)

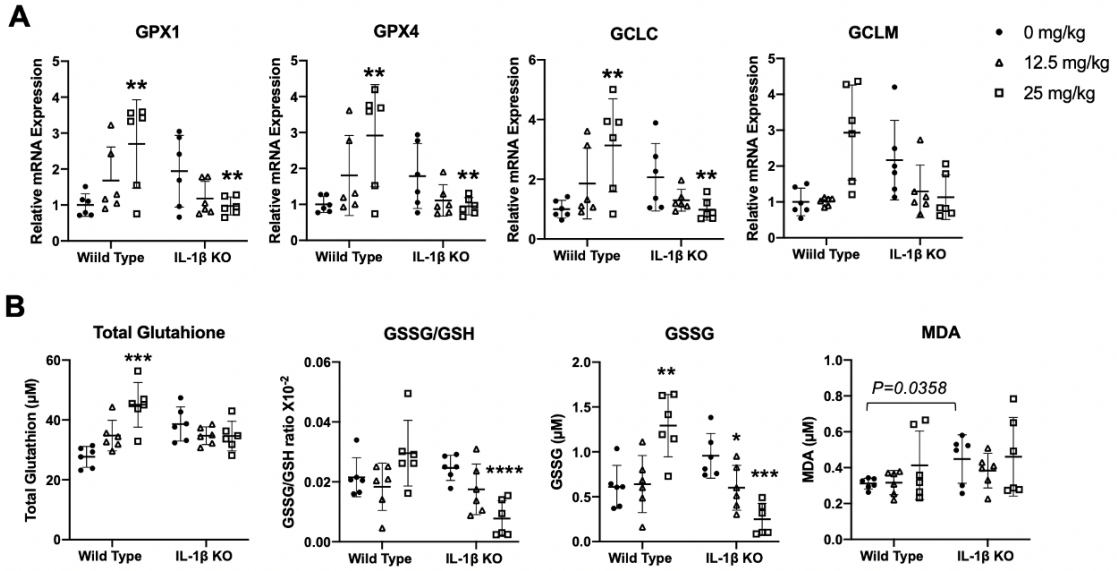

Figure 10. (A) Changes in mRNA expression levels of glutathione metabolism pathway genes: *Gpx1, Gpx4, Gclc, Gclm*. Data are mean ± SD. Statistical analyses by ANOVA followed by Dunnett's multiple comparison test (n=6, each). (B) Changes in mRNA expression levels of markers of oxidative stress in the cerebellum (total glutathione, glutathione redox ratio (GSSG/GSH) and malondialdehyde (MDA)) in the cerebral cortex of wild-type and *IL-1β* KO mice exposed to acrylamide at 0, 12.5, 25 mg/kg bw for 28 days. Data are mean±SD, n=6, each. *P< 0.05, **P<0.01, ***P<0.001, compared to the corresponding genotype control (by Dunnett's multiple comparison following ANOVA).

4.3.8 Effects of acrylamide on malondialdehyde (MDA)

Acrylamide had no effect on MDA levels in both mice genotypes (ANOVA). However, comparison of baseline data (i.e., at 0 mg acrylamide/kg bw) showed a significant difference in MDA level between wild-type and IL-1β KO mice (p= 0.0358, by Student's t-test) (Figure 10B).

4.4 DISCUSSION AND CONCLUSION

In the present study, we used *IL-1β* knockout mice to test the hypothesis that deletion of *IL-1β* protects the mice brain against acrylamide-induced neurotoxicity. This concept arose from our previous work that showed an increase in mRNA and protein expression levels of *IL-1β* in rats exposed to acrylamide at 20 mg/kg bw, as well as in BV2 murine microglia cell line (Zong et al., 2019). Surprisingly, the findings of this study suggest that deletion of *IL-1β* exacerbate the neurotoxicity of acrylamide in mice. The results of the landing foot spread test and the morphometric study demonstrated the protective role of *IL-1β* against acrylamide-induced sensorimotor dysfunction and degeneration of noradrenergic axons.

Previous *in vivo* studies reported the neuroprotective role of IL-1β in mechanically injured brain or experimental compound-induced neurodegeneration in rodents. Experimental evidence suggests that *IL-1β* promotes the survival of cortical neurons around the stab wound brain injury in mice (Abd-El-Basset et al., 2020). Furthermore, remyelination failed to occur in *IL-1β* KO mice treated with cuprizone, which induces demyelination (Mason et al., 2001). However, to the best of our knowledge, the present study is the first to demonstrate the protective role of IL-1β in environmental chemical-induced encephalopathy.

The toxic effect was especially pronounced in the 25 mg/kg bw *IL-1β* KO group, compared with the wild-type group. Splaying of the hind limbs (Figure 1) is a sign of neurotoxicity and also a sign of motor dysfunction (Mangiarini et al., 1996; Takahashi et al., 2009). Previous studies reported that the landing foot spread test is a sensitive marker of early acrylamide-induced neurotoxicity (Edwards & Parker, 1977a; Gilbert & Maurissen, 1982). Furthermore, our recent work demonstrated a clear positive association between increase in landing foot splay and monoaminergic axon degeneration in *Nrf2* KO mice (Ekuban et al., 2021).

Exposure to acrylamide also dose-dependently decreased the density of noradrenergic axon in the area of mouse somatosensory cerebral cortex. This area consists of primary somatosensory cortex (S1) of the forelimb (S1FL), hind limb (S1HL), and barrel filed (S1BF) and secondary somatosensory cortex (S2) (Davuljigari et al., 2021). The above changes were noted in *IL-1β*-KO mice but were attenuated in the wild-type (Figures 2-5), suggesting the protective role of *IL-1β* against acrylamide-induced neurodegeneration. The somatosensory cortex is responsible for processing sensory information from various parts of the body, including the face, fingers, legs, toes, and hands. The entire body is completely represented in both the SI and SII (Disbrow et al., 2000; Kaas et al., 1979; Ruben et al., 2001), highlighting the importance of the brain somatosensory cortex area. Admittedly, it is not clear at this stage whether the more profound effect of acrylamide on LFS in the *IL-1β* KO mouse (relative

to the wild-type) is due to noradrenergic axon degeneration in the somatosensory cortex area, effect of *IL-1β* deletion on peripheral nerves, or the synergistic effect of both of these pathologies, since previous studies reported that *IL-1β* plays a role in sciatic nerve regeneration (Rotshenker et al., 1992; Wu Ruoyu, 2018). Further studies are needed to determine the exact link between deletion of *IL-1β* and acrylamide-induced toxic effect on the peripheral nerves.

The results of acrylamide-induced increase in total glutathione and *Gclc* expression in wild-type mice compared with downregulation of *Gclc* in *IL-1β* KO mice suggest that the neuroprotective effect of IL-1β is mediated through glutathione synthesis. In this regard, it was reported previously that *IL-1β* can provide protection for neurons against oxidant-induced injury through enhancement of glutathione production in astrocytes (Chowdhury et al., 2018). Our findings of acrylamide-induced increase in GSSG as well as enhanced *Gpx1* and *Gpx4* expression in wild-type mice compared with decrease in GSSG and downregulation of *Gpx1* and *Gpx4* in *IL-1β* KO mice suggest that the neuroprotective effect of *IL-1β* is mediated through the enhancement of GSSG production. Our finding of acrylamide-induced upregulation of *Gpx1* and *Gpx4* in wild-type mice is in agreement with a previous study that reported increase in GPX activity in the rat brain after exposure to acrylamide by drinking water at 50 mg/300 ml for 24 hours on alternate days for 13 days (Dasari et al., 2018). Another *in vitro* study showed no accumulation of GSSG, slower clearance of H_2O_2 and increased susceptibility to peroxide-induced cell death in $GPX1^{-/-}$ mouse astrocytes treated with H_2O_2 (Liddell et al., 2006), suggesting the contribution of GPX1 to the production of GSSG and clearance of H_2O_2 in astrocytes, resulting in astrocyte survival.

Another important finding of our study was that acrylamide induced upregulation of *Nrf2* and antioxidants (*Ho-1, Nqo-1* and *Gst-m*) in wild-type mice, compared with the lack of these effects in *IL-1β* KO mice (Figure 6). However, the extent of Nrf2 activation decreased dose-dependently in wild-type mice although acrylamide had no effect on HO-1, NQO-1 and GST-M protein levels in wild-type and IL-1β KO mice. These results makes it difficult to define the role of Nrf2 pathway and related antioxidants in the observed increased susceptibility of *IL-1β* KO mice to acrylamide-induced neurotoxicity.

The present study has certain implications for occupational and environmental health and/or clinical medicine. First, the study highlighted the protective role of IL-1β in acrylamide-induced encephalopathy, by indicating that acrylamide-induced increase in IL-1β is not necessarily associated with neurotoxicity. This is useful for interpreting the rise in IL-1β in extrapolation from experimental animals to humans in risk neurotoxicity assessment of acrylamide. Second, the study implies that IL-1β inhibitors can be used carefully in treatment of patients suspected with environmental chemicals-induced encephalopathy.

The present study has also certain limitations. First, we used the cerebellum for glutathione and MDA assay as a surrogate for the cerebral cortex because of the limited amounts of samples. Although changes in the levels of glutathione and oxidized glutathione follow similar trends in the cerebrum and cerebellum after acute or subchronic exposure to the electrophile 1-bromopropane (Wang et al., 2002; Wang et al., 2003), we need to confirm that regulation of glutathione metabolism is similar in the cerebral cortex and cerebellum. Second, we did not investigate the exact mechanism of acrylamide-induced upregulation of *Gclc, Gpx1* or *Gpx4* and the role of IL-1β in this process. Third, we limited our investigation of the neuroprotective effect of IL-1β to the roles of glutathione synthesis and glutathione peroxidation; the roles of other mechanisms cannot be ruled out. Further studies are needed to clarify the above problems.

In conclusion, we have demonstrated in the present study the protective role of IL-1β against acrylamide-induced sensorimotor dysfunction and degeneration of noradrenergic axons in the somatosensory cortex of mice. This action is probably mediated through the suppression of oxidative stress by glutathione synthesis and peroxidation.

5. Chapter II: Exposure to benzo[a]pyrene decreases noradrenergic and serotonergic axons in hippocampus of mouse brain

5.1 INTRODUCTION

Millions of individuals are exposed to air pollution daily. As a result, air pollution-related morbidity and mortality continue to be significant public health concerns around the world. One of these air pollutants is benzo[a]pyrene (B[a]P), the most characterized family member of polycyclic aromatic hydrocarbons (PAHs), due to its carcinogenic effect on different organs in humans and experimental animals. B[a]P is released into a variety of environments including air, water or soil from both natural and man-made sources, such as industrial, automobile exhaust fumes and cigarette smoke (Courter et al., 2007; Kaiserman & Rickert, 1992; Wong et al., 2017). Epidemiological studies showed that neurobehavioral functions, learning ability and autonomic nervous function negatively associated with airborne benzopyrene level in coke oven workers (Niu et al., 2010; Qiu et al., 2013; Zhang et al., 2013; Zhang et al., 2008). Experimental studies showed that exposure of rats or mice to benzo(a)pyrene by intraperitoneal injection caused learning and memory deficits, anxiolytic like behavioral response and induced loss in dendritic length and number in the hippocampus (Das et al., 2019; Grova et al., 2007; Maciel et al., 2014; Qiu et al., 2011; Xia et al., 2011). Despite the above studies, the mechanism of B[a]P-induced neurotoxicity remains elusive.

The present study investigated effect of intratracheal exposure to benzopyrene, which simulates air pollution exposure, focusing on noradrenergic axons involved in cognitive function (Holland et al., 2021) and serotonergic axons involved in anxiety phenotype (Albert et al., 2014) in hippocampus of mice. In addition, the study investigated possible role of oxidative stress and inflammatory response by gene expression analysis.

5.2 MATERIAL AND METHODS

5.2.1 Chemicals

B[a]P was purchased from (A2385, Sigma Aldrich Co., LLC, St. Louis, MO), dissolved in dispersion media (DM), sonicated by bath-type sonicator, and stored in a refrigerator at 4°C. the DM was prepared as described previously (Wu et al., 2014).

5.2.2 Animals and Benzo[a]Pyrene administration

Forty-eight (9 weeks age and 21-23 gm BWT) wild-type male mice (C57BL/6J) were purchased from CLEA Japan, Inc. (Tokyo, Japan). The mice were kept under standard conditions of temperature at 21-23^{o}C, humidity (47-..%), and natural light/dark cycles of 12/12 h with food and water ad libitum. All animals were acclimatized for 1 week prior to the initiation of the experiment. Mice were weighted and randomly allocated into 4 groups (n=12/ group). Then, exposed once/week for 4 weeks to B[a]P at doses 0, 2.88, 8.67, 26.00 µg/mice (that are relevant to occupational exposure, as reviewed in (Chepelev et al., 2015) respectively, through pharyngeal aspiration under inhalation anesthesia by sevoflurane 5%. The animals were observed daily and body weight was taken 2 times/ week. All animal procedures were approved by the animal experiment committee of the Tokyo University of Science. The guidelines of Tokyo University of Science on animal experiments were strictly followed throughout the animal experiment.

5.2.3 Functional analysis test (Landing foot splay test)

The landing foot splay was performed weekly after B[a]P exposure according to the method described by (Edwards & Parker, 1977a) with little modification. Holding the mice in a horizontal position after panting his hind foot with ink, at the specified height of 15 cm dropped the mice on a soft and the distance between the fourth digits of the two hind feet was marked and measured. The test was conducted three times for each mouse and the mean of three measurements was calculated.

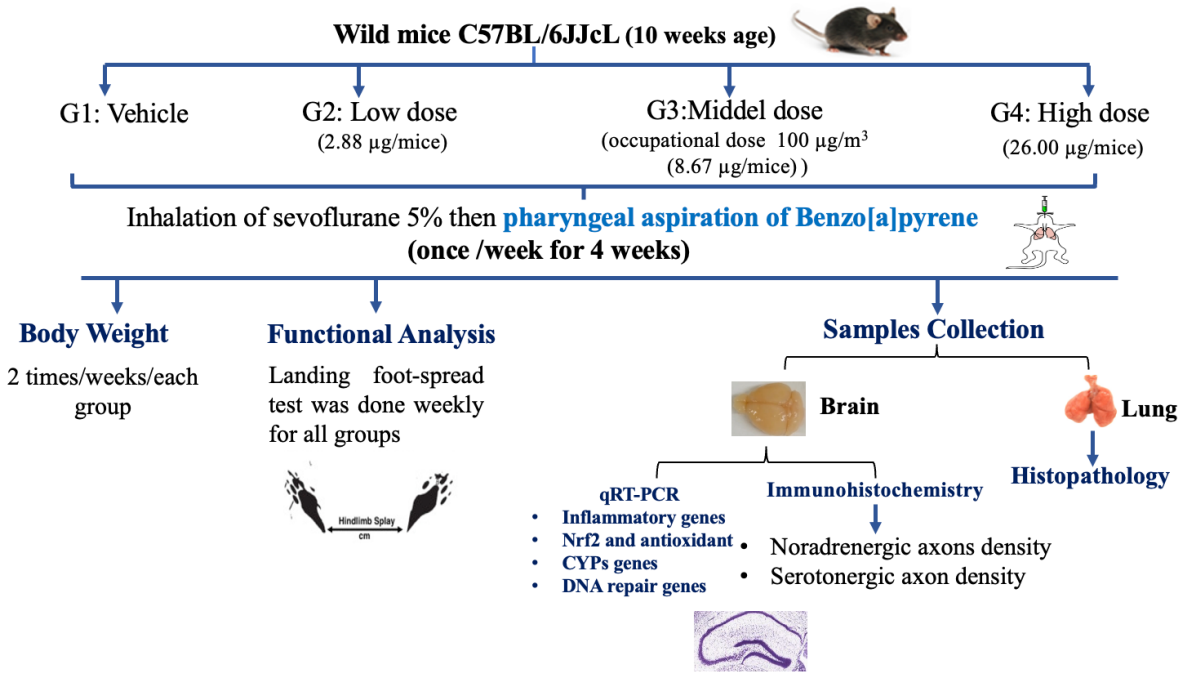

Figure 1: Schematic illustration of the experimental design. Benzo[a]pyrene is used with different concentration (0, 2.88, 8.67, 26.00 µg/mice), given by pharyngeal aspiration once/week for 4 weeks for wild type mice. The mice subjected to functional test (Landing foot spread test) after 21 days of exposure. After 4 weeks of exposure, tissue harvest is done to assess biochemical changes using mRNA expression analysis, and morphological changes using immunohistochemical staining of noradrenergic and serotonergic axons.

5.2.4 Sample collection

For histopathological analysis, four mice from each experimental groups After one week from last B[a]P exposure after one week from the last B[a]P exposure, four mice from each experimental group were anesthetized with pentobarbital sodium and infused via the left ventricle with 4% paraformaldehyde (PFA) solution for histopathological analysis. The whole brains were dissected after perfusion and fixed in 4% PFA for an overnight period. The brains were divided into three parts (forebrain, midbrain, and hindbrain) and then dried using different dilutions % of sucrose solutions 10%, 20%, and 30% for overnight period/each, respectively. Then dried midbrain samples were embedded in Tissue-Tek (optimal cutting temperature (OCT)) compound (Sakura Finetek Co., Japan) and frozen on dry ice then stored the blocks in -80°C until cryosectioning and immunohistochemistry staining. The remaining 8 mice from each experimental group were decapitation and lung and whole brains were dissected and weighted. The whole brain was placed

in a mouse brain slicer and cut into different anatomical regions which were immediately frozen on dry ice then weighted and stored at -80°C until biochemical analysis.

5.2.5 Immunohistochemistry for noradrenergic and serotonergic axon

Frozen midbrain blocks were sectioned at 40 μm thickness using a freezing microtome (Leica CM3050S, Leica Microsystems, Wetzlar, Germany). The sections were mounted on Matsunami MAS coated slides (Matsunami Glass Ind. MAS-02, Osaka, Japan) and air-dried for approximately one hour at ambient temperature then placed and stored at -80°C until immunostaining. Frozen hippocampus sections from -80°C were dried by air for 30 minutes to an hour at room temperature and then hydrated in Tris-buffered saline (TBS; 50 mM Tris, 0.15 mM NaCl, pH 7.5–7.8) for 5 min. Antigen recovery was performed using preheat Na-Citrate buffer (10 mM, pH 8.5). Sections were placed in sodium citrate buffer and kept at 80°C for 30 minutes then allowed to cool to room temperature and were washed in Tris-buffered saline with 0.01% Tween-20 (TBST). The Endogenous peroxidase activity was repressed by incubating the section for 20 min in BLOXALL® Endogenous Blocking Solution (Vector Laboratories, Inc., USA) at room temperature then sections were washed 3 times with TBST for 5 min/each. The non-specific binding sites were blocked with protein/serum block reagent at 4^{o}C overnight then continuous blocking at 37oC for 30 min in the case of noradrenergic axons were incubated for 1h at room temperature for serotonergic axons. The biotin sites were blocked by using Avidin/Biotin blocking kit (Vector laboratories, Inc., USA) in accordance with the directions provided by the manufacturer, then sections were washed 3 times with TBST for 5 min/each. The sections were incubated with primary antibody (1:1000 Mouse Anti-Noradrenaline Transporter (NAT) (Abcam, Japan) at 37°C for 2 h and 1:2000 Rabbit Anti-Serotonin Transporter (5-HT) (Immunostar, Hudson, WI) at 37°C for 48h), then sections were washed 3 times with TBST for 5 min/each. Thereafter, the sections were incubated with secondary antibody (Horse Anti-Mouse IgG antibody (H+L) Biotinylated (BA-2000, Vector Laboratories, Inc., USA) and Biotinylated Horse Anti-Rabbit IgG antibody (H+L) Biotinylated (BP-1100, Vector Laboratories, Inc., USA) for anti-NAT and anti-5-HT, respectively, for 1h at room temperature. Then, sections were washed 3 times with TBST for 5 min/each. To allowing more accessibility for binding to a biotinylated target, the sections were incubated for 45 min with VECTASTAIN® Elite® ABC Reagent, Peroxidase (Vector Laboratories, Inc., USA). The sections were stained by using ImmPACT® DAB Substrate Kit, Peroxidase (Vector Laboratories, Inc., USA) as directed by the manufacturer. Finally, sections were dried and mounted with VectaMount® AQ Aqueous Mounting

Medium (Vector Laboratories, Inc., USA) then two sections/each animal were visualized with a light microscope (Olympus, Japan). The axon length densities were quantified by using vessel analysis of Image J software (National Institute of Health, USA).

5.2.6 RNA isolation, cDNA synthesis, and quantitative polymerase chain reaction (qPCR)

Total RNA was isolated from hippocampus tissue using ReliaPrep RNA tissue miniprep system (Promega, Madison, WI) according to the manufacturer's instructions. RNA concentration and purity were determined by using a NanoDrop 2000 spectrophotometer (Thermo Scientific Inc., Waltham, MA, USA). The SuperScript III reverse transcriptase (Invitrogen, Carlsbad, CA, USA) was used for cDNA synthesis according to the manufacturer's instructions. Briefly, 4ug of total RNA was mixed with 1 µl oligo (dt) and 1 µl dNTP Mix, 5X first strand buffer, 0.1 DTT, 1 UL RNaseOUT, 1 µl SuperScript III reverse transcriptase, and the reaction was carried out as following 65°C for 5 min, 50°C for 60 min, 70°C for 15 min, and 4°C holds for 1 min. The cDNAs were then stored at 4°C until analysis. The quantitative real-time PCR was carried out to investigate the expression levels of candidate selected genes by using the THUNDERBIRD® SYBR® qPCR Mix (Toyobo Co., Osaka) on AriaMx Real-Time PCR System (Agilent Technologies, Inc., Santa Clara, CA) following the protocol of the manufacturer. The reaction conditions were performed as follows: an initial denaturation step at 95°C for 1 min, followed by an amplification step of 40 cycles at 95°C for 15 s, primer annealing at 60 °C for 30 s, extension at 72°C for 1min and a melting curve was generated after the last cycle as follow 95°C for 30 sec, 60°C for 30 sec and 95°C for 30 sec. The primer sequences of selected genes are listed in Table (1). To quantify the relative expression level of each gene, a standard curve was formed from a serial concentration of diluted cDNA samples from the control group. The relative expression level of each gene was calculated by normalization to the housekeeping gene, glyceraldehyde-3-phosphate dehydrogenase (*GAPDH*) mRNA level.

Table 1: Primers used for quantitative real-time PCR

Gene name and accession no.	Primer Sequence (5′-3′)	Amplicon size (bp)
CYP1A1 NM_001136059.2	F: ACCCTTACAAGTATTTGGTCGT R: GTCATCATGGTCATAACGTTGG	80
CYP1B1 NM_009994.2	F: TTGACCCCATAGGAAACTGC R: GCTGTCTCTTGGTAGGAGGA	113
NFKB1 NM_001410442.1	F: ATTCCGCTATGTGTGTGAAGG R: GTGACCAACTGAACGATAACC	135
TNFα NM_001278601.1	F: CAGGCGGTGCCTATGTCTC R: CGATCACCCCGAAGTTCAGTAG	89
COX-2 NM_011198.5	F: TTCGGGAGCACAACAGAGT R: TAACCGCTCAGGTGTTGCAC	148
IL-1β NM_008361.4	F: TAACCTGCTGGTGTGTGACG R: TGTCGTTGCTTGGTTCTCCT	182
IL-18 NM_001357222.1	F:TGGTTCCATGCTTTCTGGACTCCT R: TTCCTGGGCCAAGAGGAAGTGATT	132
Nlrp3 NM_145827.4	F: TCACAACTCGCCCAAGGAGGAA R: AAGAGACCACGGCAGAAGCTAG	147
Nrf2 NM_010902.5	F: GGACATGGAGCAAGTTTGGC R: TCCAGCGAGGAGATCGATGA	165
SOD-1 NM_011434.2	F: ATTGGCCGTACAATGGTGGT R: ATCCCAATCACTCCACAGGC	116
HO-1 NM_010442.2	F: AGGCTAAGACCGCCTTCCT R: TGTGTTCCTCTGTCAGCATCA	72
NQO1 NM_008706.5	F: GCAGGATTTGCCTACACATATGC R:AGTGGTGATAGAAAGCAAGGTCTTC	81
GSTM4 NM_001160411.1	F: CTGAAGGTGGAATACTTGGAGC R: GCCCAGGAACTGTGAGAAGA	63
GSTM5 NM_010360.3	F: AGAAACGGTACATCTGTGGGG R: GGATGGCGTTACTCTGGGTG	141
Msh3 NM_001311120.2	F: TGCAAGCATACCTACCCACAGA R: CGGCAGTTTCAGTTTGCTTCAC	95
Ddb1 NM_015735.3	F: TGCAGTGGAGATCTTGGATGATG R: TTGACAAACTCGCCCAGGTG	150
Ercc1 NM_007948.2	F: CTGGAGACCTACAAGGCGTATG R: GATTTCACGGTGGTCAGACACTC	107
GAPDH NM_001289726.2	F: GCCTGGAGAAACCTGCCAA R: TGAAGTCGCAGGAGACAACC	117

5.2.7 Statistical analysis

The results were analyzed with GraphPad Prism 8 (GraphPad Software, La Jolla, CA) and JMP Pro 14.0 also was used to analyze the data (SAS Institute Inc., Cary, NC, USA). The data were presented as the mean ± SD. Significant differences between treatment groups and the control one

and among all groups were determined using one-way ANOVA followed by Dunnett's test. The significance level was set as $p < 0.05$.

5.3 RESULTS

5.3.1 Body, brain weight and functional analysis test

B[a]P exposure for 4 weeks period did not affect body weight, irrespective of dose. Likewise, there was no change in the brain weights relative to body weights in the treated groups compared with the control group. Landing foot spread distance showed a slight increase in the third and fourth weeks of B[a]P exposure in all treated groups (Fig. 2).

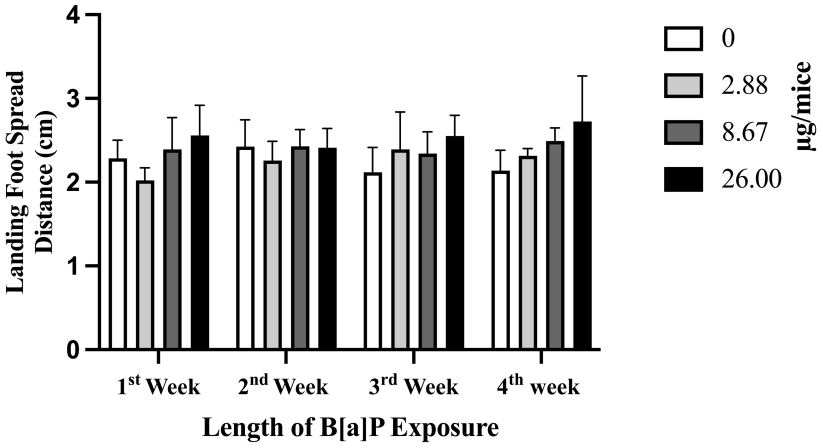

Fig. 2 Effect of exposure to benzo[a]pyrene on landing foot spread distance. Data are mean ± SD

5.3.2 Quantification of noradrenergic and serotonergic axons

As the hippocampus plays a curial role in regulating learning, memory encoding, memory consolidation, and spatial navigation. The density of noradrenergic and serotonergic axons length was quantified in the hippocampal cornu ammonis (CA1) and (CA3) regions as shown in (Fig. 3A and 3B). The density of noradrenergic axons significantly reduced in the hippocampal CA1 area for all B[a]P treated groups (Fig. 3A). Moreover, noradrenergic axons density of CA3 hippocampal area showed a reduction in the high treated group and a significant reduction in low and middle B[a]P treated groups compared with a control group (Fig. 3B).

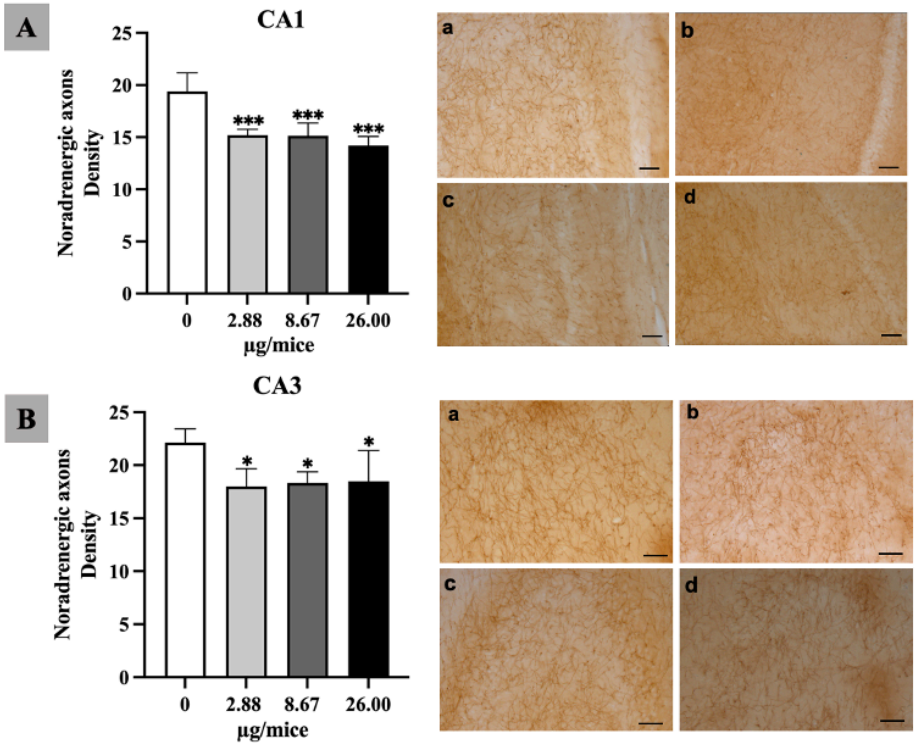

Fig. 3 Effect of exposure to B[a]P on density of noradrenergic axons in hippocampal CA1(A) and CA3 (B) area. Control group (a), group exposed to low (b), middle (c), and high dose (d). Scale bars = 40 µm. Data are mean ± SD. *$p < 0.05$ and ** $p < 0.01$.

B[a]P exposure induced a slight reduction in the density of serotonergic axon and this reduction was significant in high dose treated group compared with control in both CA1 and CA3 hippocampal regions ($p < 0.01$ and $p < 0.05$) as indicated in Fig. (4A and 4B).

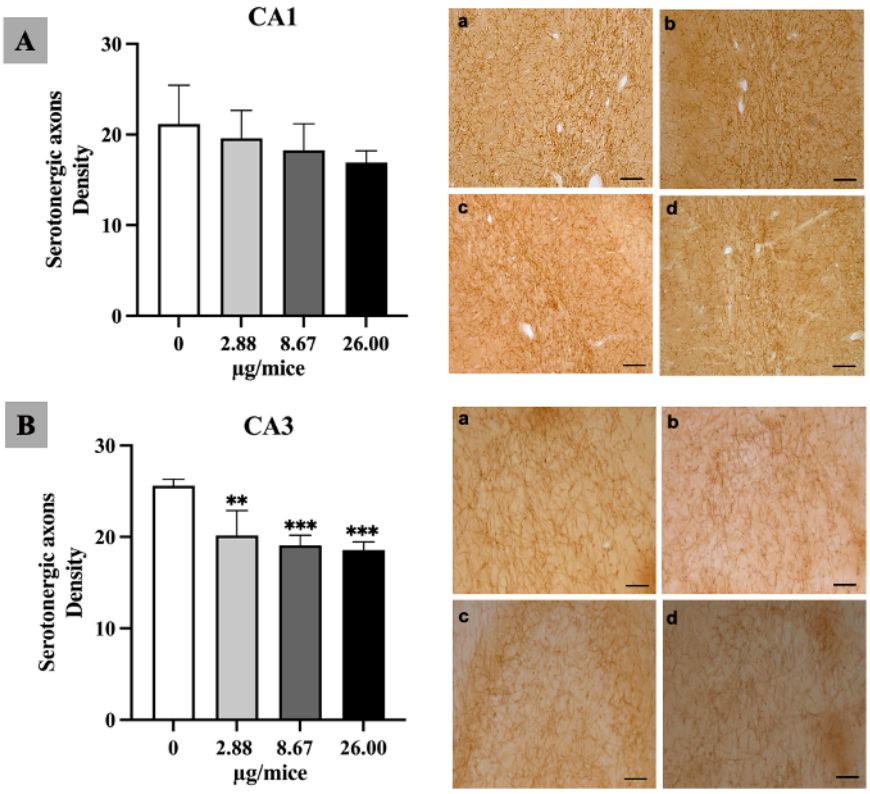

Fig. 4 Effect of exposure to B[a]P on the density of serotonergic axons in hippocampal CA1(A) and CA3 (B) area. Control group (a), group exposed to low (b), middle (c), and high dose (d). Scale bars = 40 µm. Data are mean ± SD and Statistical significance: *p < 0.05 and ** p < 0.01.

5.3.3 The expression levels of selected mRNA

In the current study, the effect of B[a]P exposure on the expression of genes involved in B[a]P metabolism, Pro-inflammatory cytokines, and inflammatory mediator genes, *Nrf2* and its downstream antioxidant genes and genes involved in the DNA repair process in mice hippocampus tissue was quantified using quantitative real-time PCR. In comparison to the control group, the B[a]P-treated groups showed a change in expression levels of studied genes after 4 weeks of exposure (Fig. 5, 6, 7, and 8).

As *CYP1A1* and *CYP1B1* genes are essential and play a crucial role in the oxidation and metabolism of B[a]P to its metabolite. B[a]P induced *CYP1A1* and *CYP1B1* mRNA expression hippocampus tissue. *CYP1A1* expression level was revealed increase in all B[a]P treated groups with a significant (P<0.001) upregulated (2.545±0.74) in the high dose treated group compared with

the control. *CYP1B1* expression level showed a slight increase in low, and middle-treated groups (Fig. 5 a and b).

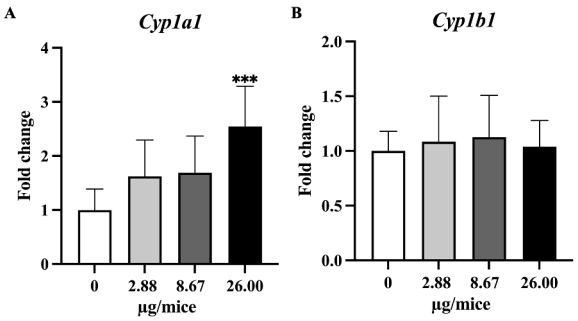

Fig. 5 Relative hippocampal expression levels genes involve in B[a]P metabolism. a: *CYP1A1* and b*: CYP1B1*. Data were presented as the mean ± SD and statistical significance: *p < 0.05 and *** p < 0.001.

The finding results indicated that B[a]P has the ability to promote the expression of inflammatory factors in hippocampal tissue (Fig. 6). B[a]P exposure significantly up-regulate *TNFα* mRNA levels in both middle and high doses compared with control. *TNFα, IL-1β* and *IL-18* mRNA levels showed the highest and significant (P<0.001, P<0.05) up-regulation (4.64±1.59,1.70±0.41, and 1.35±0.32, respectively) in the group exposed to a high dose of B[a]P (Fig.6a, b, and c). Moreover, the *TNFα* expression level was significant (P<0.01) up-regulated (3.38±2.01) in the group of middle dose relative to control. There were also significant differences in *TNFα* mRNA levels between the high and middle-treated group compared with the group exposed to low dose (Fig.6a). likewise, *IL-1β* revealed significant differences between high treated group compared with group exposed to the middle dose (Fig.6b). Low B[a]P treated group showed a significant (P<0.05) increase of *NLRP3* and *IL-18* mRNA expression levels (2.03±0.81 and 1.38±0.28) and increase of *IL-1β, COX-2* and *NFKB1* mRNA relative to control group as shown in Fig. (6 b, c, d, e, and f). Besides, the *COX-2* and *NFKB1* mRNA showed an increase in expression levels in middle and high groups relative to control one (Fig. 6d and e).

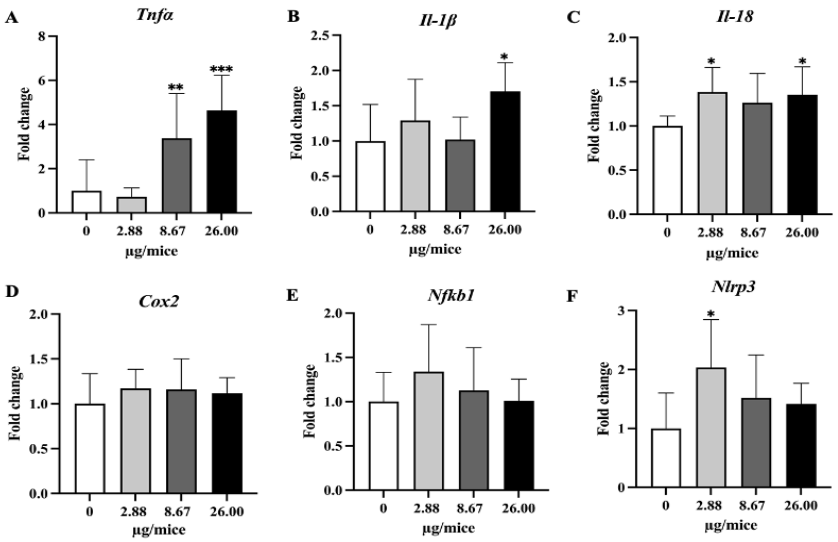

Fig. 6 Relative hippocampal expression levels of Pro-inflammatory cytokines and inflammatory mediator. a: *TNFα*, b: *IL-1β*, c: *IL-18*, d: *COX-2*, e: *NFKB1* and f: *NLRP3.* Data were presented as the mean ± SD and statistical significance: *p < 0.05, **p < 0.01, and *** p <0.001.

B[a]P exposure revealed minor disturbed expression of *Nrf2* and antioxidant genes in hippocampal tissue (Fig. 7), where expression levels of *Nrf2*, *Ho-1,* and *NQO1* declined (0.91±0.12, 0.93±0.18, and 0.80±0.23), respectively, especially in high dose treated groups (Fig.7 a, c, and d). *SOD1* and *NQO1* mRNA also decline (0.89±0.18 and 0.91±0.42) in the middle dose treated group compared with control ones (Fig.7 b and d). However, the expression of *GSTM5* was increased (1.11±0.30, 1.08±0.23, and 1.19±0.14) in low, middle, and high dose treated groups, respectively relative to the control (Fig. 7f).

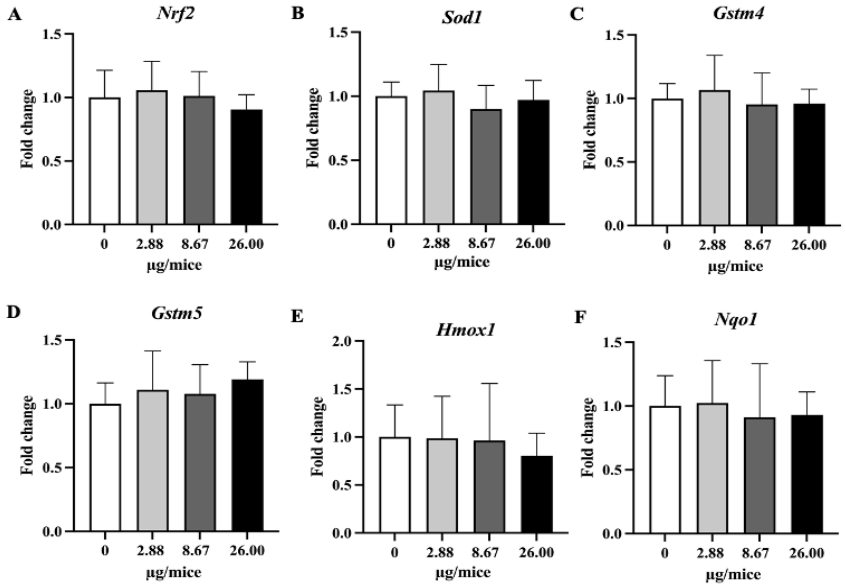

Fig. 7 Relative hippocampal expression levels of *Nrf2* and its downstream antioxidant genes. a: *Nrf2*, b: *SOD1*, c: *HO-1*, d: *NQO1*, e: *GSTM4* and f: *GSTM5* mRNAs. Data were presented as the mean ± SD.

The same pattern of expression was observed in DNA repair genes (*MSH3*, *Ddb1,* and *ERCC1*). The DNA repair gene expression levels were lower in all groups exposed to different doses of B[a]P relative to control ones. The lowest levels were in the group exposed to the high dose of B[a]P (0.77± 0.15, 0.80±0.10 and 0.84±0.09) as shown in Fig. (8 a, b and c).

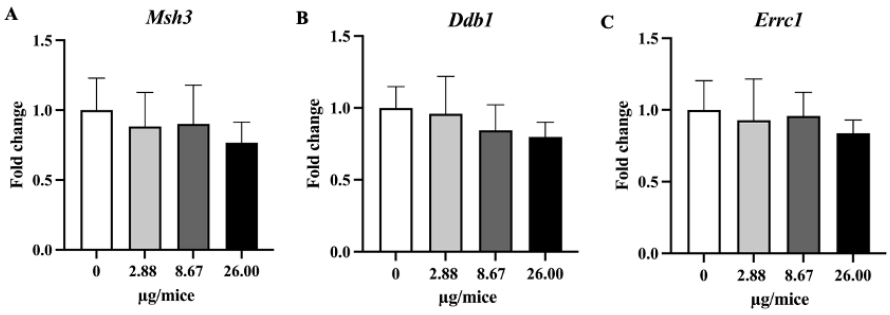

Fig.8 Relative hippocampal expression levels of genes involved in *DNA repair process*. a: *MSH3*, b: *Ddb1*, c: *ERCC1* mRNAs. Data were presented as the mean ± SD.

5.4 DISCUSSION AND CONCLUSION

The study demonstrated that exposure to B[a]P reduced the density of noradrenergic axons in CA1 and CA3 and serotonergic axons in CA3 in the hippocampus of mice. Exposure to B[a]P upregulated gene expression of *Cyp1a1*, *Tnfα*, *Il-1β* and *Il-18* largely in a dose-dependent manner and that of *Nlrp3* only at low exposure level, while did not change expression of examined antioxidative genes. The study reveals adverse effect of B[a]P on noradrenergic and serotonergic axons in the hippocampus of mice and suggests involvement of inflammatory pathway with neurotoxicity of B[a]P.

A previous study using Golgi staining showed that exposure to B[a]P induced loss in dendritic length and number in the hippocampus in adult rats, but it did not specify type of affected axons (Das et al., 2019). Our study revealed that exposure to B[a]P decreased noradrenergic and serotonergic axons in CA1 or CA3 region of hippocampus, and noradrenergic axons were more susceptible to B[a]P exposure than serotonergic axons in CA1 region of hippocampus in mice.

The hippocampus is known to play a pivotal role in learning and memory processes (Lynch, 2004; Varallyay et al., 2013). In Alzheimer disease, there is significant loss of locus coeruleus noradrenergic neurons projecting to the hippocampus (Holland et al., 2021). On the other hand, decreased serotonergic activity has been implicated with anxiety and major depression (Albert et al., 2014). The result on noradrenergic axons should be noted as epidemiological studies show negative association between B[a]P exposure and learning ability (Niu et al., 2010; Qiu et al., 2013; Zhang et al., 2013; Zhang et al., 2008) and experimental studies show that exposure to B[a]P induces learning and memory impairment (Das et al., 2019; Grova et al., 2007; Maciel et al., 2014; Qiu et al., 2011; Xia et al., 2011).

Greater susceptibility of noradrenergic axons than serotonergic axons in CA1 region might be related with a previous study which shows exposure to B[a]P by intraperitoneal injection at 50 mg/kg bw decreased the level of NA, DA or DOPAC but did not induce major alteration in 5-HT or 5-HIAA, and the most important change in midbrain was decrease in NA (Stephanou et al., 1998).

In the present study, exposure to B[a]P upregulated expression of proinflammatory cytokines (*Tnfα, Il-1β* and *Il-18*) and *Nlrp3*. A previous study showed that exposure to B[a]P at

1mg/kg bw by intraperitoneal injection for 2 months upregulated gene expression of *Tnfα*, but downregulated that of *IL-1β* in wild-type mice (D. Liu et al., 2020). It is possible that the level of gene expression of *Il-1β* depends on exposure duration or level. In this regard, B[a]P-induced production of IL-1β is demonstrated by an in vitro study that exposure of mouse microglia BV2 cells to B[a]P at 10 μM resulted in production of pro-inflammatory factors, including nitric oxide, IL-1β, and IL-6, iNOS and COX-2 (Bao et al., 2019).

On the other hand, the expression of Nrf2-dependent antioxidant genes in the hippocampus was not affected by B[a]P exposure in the present study. A previous study (Saunders et al., 2006) showed that exposure to B[a]P by gavage at 25 mg/kg bw or more inhibited the activity of superoxide dismutase and glutathione peroxidase, and increased catalase activity and lipid peroxidation, suggesting production of oxidative stress, but it should be noted that the exposure level was far higher compared to the present study. The present study shows that exposure to B[a]P upregulates expression of proinflammatory cytokine genes but does not upregulate antioxidative genes, suggesting greater role of inflammatory pathway than oxidative stress in B[a]P-induced neurodegeneration at low exposure level.

After B[a]P enters the body, it binds with AhR and enhances the expression of CYP P450 genes which metabolize the B[a]P into benzo(a)pyrene-7,8- epoxides that are further hydrated into diol epoxides, which are very active metabolites, by epoxide hydrolase (Fujii-Kuriyama & Mimura, 2005; Ramadoss et al., 2005; Yang et al., 1977) In the present study, *Cyp1a1* expression level was significantly upregulated at 26 μg/mice, while *Cyp1b1* didn't show high alterations in its expression. The brain is one of the extrahepatic tissues that express CYP1A1 both constitutively and following induction (Iba et al., 2003; Strobel et al., 2001). In a recent study, exposure to B[a]P by oral gavage at 20 and 200 mg/kg for 11 consecutive days induced significant overexpression of *Cyp1a1/Cyp1b1* in the frontal cortex, temporal cortex, and hippocampus regions of mouse brains (Cherif, 2021). The difference in the result of *Cyp1b1* between the previous study and the present study might be due to the difference in exposure level.

Exposure to B[a]P once per week for 4 weeks did not affect body weight and brain weight, irrespective of exposure level. The result on body weight is in agreement with a previous study [26] which reports that exposure to B[a]P at 0.02–200 mg/kg/day for 11 days has no effect on

body weight. However, the result of brain weight is different from a previous study which shows that exposure to B[a]P by intraperitoneal injection at 3.2 and 7.8 mg/kg bw decreases the brain weight (Tu et al., 2004). The discrepancies between the present study and the previous study might be due to differences in exposure level, and duration of treatment.

In conclusion, exposure to B[a]P decreases the density of noradrenergic and serotonergic axons. Upregulation of proinflammatory cytokines may contribute to the neurotoxicity of B[a]P, but further studies are needed to understand fully the mechanism of toxicity.

6. REFERENCES

Abd-El-Basset, E. M., Rao, M. S., & Alsaqobi, A. (2020). Interferon-Gamma and Interleukin-1Beta Enhance the Secretion of Brain-Derived Neurotrophic Factor and Promotes the Survival of Cortical Neurons in Brain Injury. *Neurosci Insights*, *15*, 2633105520947081. https://doi.org/10.1177/2633105520947081

Acaroz, U., Ince, S., Arslan-Acaroz, D., Gurler, Z., Kucukkurt, I., Demirel, H. H., Arslan, H. O., Varol, N., & Zhu, K. (2018). The ameliorative effects of boron against acrylamide-induced oxidative stress, inflammatory response, and metabolic changes in rats. *FCT*, *118*, 745-752. https://doi.org/10.1016/j.fct.2018.06.029

Albert, P. R., Vahid-Ansari, F., & Luckhart, C. (2014). Serotonin-prefrontal cortical circuitry in anxiety and depression phenotypes: pivotal role of pre- and post-synaptic 5-HT1A receptor expression. *Front Behav Neurosci*, *8*, 199. https://doi.org/10.3389/fnbeh.2014.00199

An, L., Li, G., Si, J., Zhang, C., Han, X., Wang, S., Jiang, L., & Xie, K. (2016). Acrylamide Retards the Slow Axonal Transport of Neurofilaments in Rat Cultured Dorsal Root Ganglia Neurons and the Corresponding Mechanisms. *Neurochemical Research*, *41*(5), 1000-1009. https://doi.org/10.1007/s11064-015-1782-z

Anderson, C. M., & Swanson, R. A. (2000). Astrocyte glutamate transport: Review of properties, regulation, and physiological functions. *Glia*, *32*(1), 1-14. <Go to ISI>://WOS:000089634200001

Backe, W. J., Yingling, V., & Johnson, T. (2014). The determination of acrylamide in environmental and drinking waters by large-volume injection - hydrophilic-interaction liquid chromatography and tandem mass spectrometry. *Journal of Chromatography A*, *1334*, 72-78. https://doi.org/10.1016/j.chroma.2014.02.005

Bao, Y., Chen, Q., Xie, Y., Tao, Z., Jin, K., Chen, S., Bai, Y., Yang, J., & Shan, S. (2019). Ferulic acid attenuates oxidative DNA damage and inflammatory responses in microglia induced by benzo(a)pyrene. *Int Immunopharmacol*, *77*, 105980. https://doi.org/10.1016/j.intimp.2019.105980

Barnes, J. L., Zubair, M., John, K., Poirier, M. C., & Martin, F. L. (2018). Carcinogens and DNA damage. *Biochemical Society Transactions*, *46*, 1213-1224. https://doi.org/10.1042/Bst20180519

Benveniste, E. (1992). Cytokines: influence on glial cell gene expression and function. pp 106 – 153 Basel: Karger. .

Berenblum, I. (1945). 3-4-Benzpyrene from Coal Tar. *Nature*, *156*(3968), 601-601. https://doi.org/DOI 10.1038/156601a0

Bezza, F. A., & Chirwa, E. M. N. (2017). The role of lipopeptide biosurfactant on microbial remediation of aged polycyclic aromatic hydrocarbons (PAHs)-contaminated soil. *Chemical Engineering Journal*, *309*, 563-576. https://doi.org/10.1016/j.cej.2016.10.055

Bin-Jumah, M., Abdel-Fattah, A. M., Saied, E. M., El-Seedi, H. R., & Abdel-Daim, M. M. (2021). Acrylamide-induced peripheral neuropathy: manifestations, mechanisms, and potential treatment modalities. *ESPR*, *28*(11), 13031-13046. https://doi.org/10.1007/s11356-020-12287-6

Block, M. L., Zecca, L., & Hong, J. S. (2007). Microglia-mediated neurotoxicity: uncovering the molecular mechanisms. *Nature Reviews Neuroscience*, *8*(1), 57-69. https://doi.org/10.1038/nrn2038

Bogdanovic, T., Pleadin, J., Petricevic, S., Listes, E., Sokolic, D., Markovic, K., Ozogul, F., & Simat, V. (2019). The occurrence of polycyclic aromatic hydrocarbons in fish and meat products of Croatia and dietary exposure. *Journal of Food Composition and Analysis*, *75*, 49-60. https://doi.org/10.1016/j.jfca.2018.09.017

Borgen, A., Darvey, H., Castagnoli, N., Crocker, T. T., Rasmussen, R. E., & Wang, I. Y. (1973). Metabolic conversion of benzo(a)pyrene by Syrian hamster liver microsomes and binding of metabolites to deoxyribonucleic acid. *J Med Chem*, *16*(5), 502-506. https://doi.org/10.1021/jm00263a020

Bostrom, C. E., Gerde, P., Hanberg, A., Jernstrom, B., Johansson, C., Kyrklund, T., Rannug, A., Tornqvist, M., Victorin, K., & Westerholm, R. (2002). Cancer risk assessment, indicators, and guidelines for polycyclic aromatic hydrocarbons in the ambient air. *Environmental Health Perspectives*, *110*, 451-488. https://doi.org/DOI 10.1289/ehp.02110s3451

Brandt, H. C. A., & Watson, W. P. (2003). Monitoring human occupational and environmental exposures to polycyclic aromatic compounds. *Annals of Occupational Hygiene*, *47*(5), 349-378. https://doi.org/10.1093/annhyg/meg052

Brown L, R. M., Hill D, Bancroft KCC. (1982). Qualitative and quantitative studies on the in situ adsorption, degradation and toxicity of acrylamide by the spiking of the waters of two sewage works and a river. *Water Research*, *16*, 579–591. https://doi.org/doi: 10.1016/0043- 135490078- 1

Bukowska, B. (2015). Hemoglobin adducts as biomarkers of human exposure to selected xenobiotics. *Postepy Higieny I Medycyny Doswiadczalnej*, *69*, 668-680. https://doi.org/Doi 10.5604/17322693.1156936

Bukowska, B., & Sicinska, P. (2021). Influence of Benzo(a)pyrene on Different Epigenetic Processes. *International Journal of Molecular Sciences*, *22*(24). https://doi.org/ARTN 13453

10.3390/ijms222413453

Checker, R., Patwardhan, R. S., Sharma, D., Menon, J., Thoh, M., Bhilwade, H. N., Konishi, T., & Sandur, S. K. (2012). SchisandrinBexhibits anti-inflammatory activity through modulation of the redox-sensitive transcription factors Nrf2 and NF-κB. *Free Radic. Biol. Med.*, *53*, 1421-1430.

Chen, W., Shen, Y., Su, H. M., & Zheng, X. D. (2014). Hispidin derived from Phellinus linteus affords protection against acrylamide-induced oxidative stress in Caco-2 cells. *Chemico-Biological Interactions*, *219*, 83-89. https://doi.org/10.1016/j.cbi.2014.05.010

Chen, Z. C., & Zhong, C. J. (2014). Oxidative stress in Alzheimer's disease. *Neuroscience Bulletin*, *30*(2), 271-281. https://doi.org/10.1007/s12264-013-1423-y

Chepelev, N. L., Moffat, I. D., Bowers, W. J., & Yauk, C. L. (2015). Neurotoxicity may be an overlooked consequence of benzo[a]pyrene exposure that is relevant to human health risk assessment. *Mutation Research-Reviews in Mutation Research*, *764*, 64-89. https://doi.org/10.1016/j.mrrev.2015.03.001

Cherif, L. S., Cao-Lei, L., Farinelle, S., Muller, C. P., Turner, J. D., Schroeder, H., & Grova, N. (2021). Assessment of 9-OH- and 7,8-diol-benzo[a]pyrene in Blood as Potent Markers of Cognitive Impairment Related to benzo[a]pyrene Exposure: An Animal Model Study. *Toxics*, *9* (3).

Chowdhury, T., Allen, M. F., Thorn, T. L., He, Y., & Hewett, S. J. (2018). Interleukin-1beta Protects Neurons against Oxidant-Induced Injury via the Promotion of Astrocyte

Glutathione Production. *Antioxidants (Basel)*, *7*(8). https://doi.org/10.3390/antiox7080100

Chung, C., Kim, T., Kim, M., Kim, M., Song, H., Kim, T. S., Seo, E., Lee, S. H., Kim, H., & Kim, S. K. e. (2013). Hippo-Foxa2signaling pathway plays a role in peripheral lung maturation and surfactant homeostasis. *Proc. Natl. Acad. Sci.*, *110*, 7732-7737.

Chung, J. Y., Kim, J. Y., Kim, Y. J., Jung, S. J., Park, J. E., Lee, S. G., Kim, J. T., Oh, S., Lee, C. J., Yoon, Y. D., Yoo, Y. H., & Kim, J. M. (2007). Cellular Defense mechanisms against benzo[a] pyrene in testicular leydig cells: Implications of p53, aryl-hydrocarbon receptor, and cytochrome p450 1A1 status. *Endocrinology*, *148*(12), 6134-6144. https://doi.org/10.1210/en.2007-0006

Courter, L. A., Pereira, C., & Baird, W. M. (2007). Diesel exhaust influences carcinogenic PAH-induced genotoxicity and gene expression in human breast epithelial cells in culture. *Mutat Res*, *625*(1-2), 72-82. https://doi.org/10.1016/j.mrfmmm.2007.05.005

Czeh, M., Gressens, P., & Kaindl, A. M. (2011). The Yin and Yang of Microglia. *Developmental Neuroscience*, *33*(3-4), 199-209. https://doi.org/10.1159/000328989

da Silva, A. I., Galindo, L. C. M., Nascimento, L., Freitas, C. M., Manhaes-de-Castro, R., Lagranha, C. J., & de Souza, S. L. (2014). Fluoxetine treatment of rat neonates significantly reduces oxidative stress in the hippocampus and in behavioral indicators of anxiety later in postnatal life. *Canadian Journal of Physiology and Pharmacology*, *92*(4), 330-337. https://doi.org/10.1139/cjpp-2013-0321

Das, L., Patel, B., & Patri, M. (2019). Adolescence benzo[a]pyrene treatment induces learning and memory impairment and anxiolytic like behavioral response altering neuronal morphology of hippocampus in adult male Wistar rats. *Toxicol Rep*, *6*, 1104-1113. https://doi.org/10.1016/j.toxrep.2019.10.014

Dasari, S., Muni Swamy, G., Sailaja, G., Keerthi, R., Prabhakar Yellanur, K., & Balaji, M. (2018). Assessment of biomarkers in acrylamide-induced neurotoxicity and brain histopathology in rat

. *Journal of Applied Biology & Biotechnology*, *6(06)*, 79-86.

Davuljigari, C. B., Ekuban, F. A., Zong, C., Fergany, A. A. M., Morikawa, K., & Ichihara, G. (2021). Nrf2 Activation Attenuates Acrylamide-Induced Neuropathy in Mice. *International Journal of Molecular Sciences*, *22*(11). https://doi.org/ARTN 5995 10.3390/ijms22115995

Dejchanchaiwong, R., Tekasakul, P., Tekasakul, S., Phairuang, W., Nim, N., Sresawasd, C., Thongboon, K., Thongyen, T., & Suwattiga, P. (2020). Impact of transport of fine and ultrafine particles from open biomass burning on air quality during 2019 Bangkok haze episode. *Journal of Environmental Sciences*, *97*, 149-161. https://doi.org/10.1016/j.jes.2020.04.009

Dheen, S. T., Kaur, C., & Ling, E. A. (2007). Microglial activation and its implications in the brain diseases. *Current Medicinal Chemistry*, *14*(11), 1189-1197. https://doi.org/Doi 10.2174/092986707780597961

Disbrow, E., Roberts, T., & Krubitzer, L. (2000). Somatotopic organization of cortical fields in the lateral sulcus of Homo sapiens: Evidence for SII and PV. *Journal of Comparative Neurology*, *418*(1), 1-21. https://doi.org/Doi 10.1002/(Sici)1096-9861(20000228)418:1<1::Aid-Cne1>3.0.Co;2-P

Edwards, P. M., & Parker, V. H. (1977a). A simple, sensitive, and objective method for early assessment of acrylamide neuropathy in rats. *Toxicol Appl Pharmacol*, *40*(3), 589-591. https://doi.org/10.1016/0041-008x(77)90083-7

Edwards, P. M., & Parker, V. H. (1977b). A simple, sensitive, and objective method for early assessment of acrylamide neuropathy in rats. *Toxicol. Appl. Pharmacol*, *40*(3), 589-591. https://doi.org/10.1016/0041-008x(77)90083-7

Ekuban, F. A., Zong, C., Takikawa, M., Morikawa, K., Sakurai, T., Ichihara, S., Itoh, K., Yamamoto, M., Ohsako, S., & Ichihara, G. (2021). Genetic ablation of Nrf2 exacerbates neurotoxic effects of acrylamide in mice. *Toxicology*, *456*. https://doi.org/ARTN 152785 10.1016/j.tox.2021.152785

Elmore, J. S., Koutsidis, G., Dodson, A. T., Mottram, D. S., & Wedzicha, B. L. (2005). The effect of cooking on acrylamide and its precursors in potato, wheat and rye. *Chemistry and Safety of Acrylamide in Food*, *561*, 255-269. <Go to ISI>://WOS:000232360300019

Erkekoglu, P., & Baydar, T. (2010). Toxicity of acrylamide and evaluation of its exposure in baby foods. *Nutrition Research Reviews*, *23*(2), 323-333. https://doi.org/10.1017/S0954422410000211

Europe.2020., A. Q. i. Available online: https://www.eea.europa.eu/publications/air-quality-in-europe-2020-report (accessed on 12 May 2022).

Exon, J. H. (2006). A review of the toxicology of acrylamide. *J Toxicol Environ Health B Crit Rev*, *9*(5), 397-412. https://doi.org/10.1080/10937400600681430

Foyet, H. S., Tchinda Deffo, S., Koagne Yewo, P., Antioch, I., Zingue, S., Asongalem, E. A., Kamtchouing, P., & Ciobica, A. (2017). Ficus sycomorus extract reversed behavioral impairment and brain oxidative stress induced by unpredictable chronic mild stress in rats. *BMC Complement Altern Med*, *17*(1), 502. https://doi.org/10.1186/s12906-017-2012-9

Friedman, M. (2003). Chemistry, biochemistry, and safety of acrylamide. A review. *Journal of Agricultural and Food Chemistry*, *51*(16), 4504-4526. https://doi.org/10.1021/jf030204+

Fujii-Kuriyama, Y., & Mimura, J. (2005). Molecular mechanisms of AhR functions in the regulation of cytochrome P450 genes. *Biochem Biophys Res Commun*, *338*(1), 311-317. https://doi.org/10.1016/j.bbrc.2005.08.162

Gharby, S., Harhar, H., Farssi, M., Taleb, A. A., Guillaume, D., & Laknifli, A. (2018). Influence of roasting olive fruit on the chemical composition and polycyclic aromatic hydrocarbon content of olive oil. *Ocl-Oilseeds and Fats Crops and Lipids*, *25*(3). https://doi.org/ARTN A303 10.1051/ocl/2018013

Gilbert, S. G., & Maurissen, J. P. J. (1982). Assessment of the Effects of Acrylamide, Methylmercury, and 2,5-Hexanedione on Motor Functions in Mice. *Journal of Toxicology and Environmental Health*, *10*(1), 31-41. https://doi.org/Doi 10.1080/15287398209530228

Grova, N., Valley, A., Turner, J. D., Morel, A., Muller, C. P., & Schroeder, H. (2007). Modulation of behavior and NMDA-R1 gene mRNA expression in adult female mice after sub-acute administration of benzo(a)pyrene. *Neurotoxicology*, *28*(3), 630-636. https://doi.org/10.1016/j.neuro.2007.01.010

Hawley GG, L. R. (1997). Hawley's condensed chemical dictionary. *Van Nostrand Reinhold*.

Hewett, S. J., Jackman, N. A., & Claycomb, R. J. (2012). Interleukin-1beta in Central Nervous System Injury and Repair. *Eur. J.Neurodegener. Dis*, *1*(2), 195-211. https://www.ncbi.nlm.nih.gov/pubmed/26082912

Holland, N., Robbins, T. W., & Rowe, J. B. (2021). The role of noradrenaline in cognition and cognitive disorders. *Brain*, *144*(8), 2243-2256. https://doi.org/10.1093/brain/awab111

IARC, Group, W., & Benzo[a]Pyrene. (2010). Iarc Monographs on the Identification of Carcinogenic Hazards to Humans. . Available online: https://monographs.iarc.who.int/wp-content/uploads/2018/06/mono100F-14.pdf (accessed on 12 May 2022).

Iba, M. M., Storch, A., Ghosal, A., Bennett, S., Reuhl, K. R., & Lowndes, H. E. (2003). Constitutive and inducible levels of CYP1A1 and CYP1A2 in rat cerebral cortex and cerebellum. *Arch Toxicol*, *77*(10), 547-554. https://doi.org/10.1007/s00204-003-0488-1

Innamorato, N. G., Jazwa, A., Rojo, A. I., Garcia, C., Fernandez-Ruiz, J., Grochot-Przeczek, A., Stachurska, A., Jozkowicz, A., Dulak, J., & Cuadrado, A. (2010). Different Susceptibility to the Parkinson's Toxin MPTP in Mice Lacking the Redox Master Regulator Nrf2 or Its Target Gene Heme Oxygenase-1. *Plos One*, *5*(7). https://doi.org/ARTN e11838 10.1371/journal.pone.0011838

Innamorato, N. G., Rojo, A. I., Garcia-Yague, A. J., Yamamoto, M., de Ceballos, M. L., & Cuadrado, A. (2008). The transcription factor Nrf2 is a therapeutic target against brain inflammation. *Journal of Immunology*, *181*(1), 680-689. https://doi.org/DOI 10.4049/jimmunol.181.1.680

Ishihara, K., Matsunaga, A., Miyoshi, T., Nakamura, K., Nakayama, T., Ito, S., & Koga, H. (2005). Formation of acrylamide in a processed food model system, and examination of inhibitory conditions. *Journal of the Food Hygienic Society of Japan*, *46*(2), 33-39. https://doi.org/DOI 10.3358/shokueishi.46.33

Jiang, Y. M., Wang, Y., Tan, H. S., Yu, T., Fan, X. M., Chen, P., Zeng, H., Huang, M., & Bi, H. C. (2016). Schisandrol B protects against acetaminophen-induced acute hepatotoxicity in mice via activation of the NRF2/ARE signaling pathway. *Acta Pharmacologica Sinica*, *37*(3), 382-389. https://doi.org/10.1038/aps.2015.120

Kaas, J. H., Nelson, R. J., Sur, M., Lin, C. S., & Merzenich, M. M. (1979). Multiple Representations of the Body within the Primary Somatosensory Cortex of Primates. *Science*, *204*(4392), 521-523. https://doi.org/DOI 10.1126/science.107591

Kaiserman, M. J., & Rickert, W. S. (1992). Carcinogens in tobacco smoke: benzo[a]pyrene from Canadian cigarettes and cigarette tobacco. *Am J Public Health*, *82*(7), 1023-1026. https://doi.org/10.2105/ajph.82.7.1023

Kamalabadi, M., Kamankesh, M., Mohammadi, A., Hadian, Z., & Ferdowsi, R. (2020). Contamination and Daily Intake of Polycyclic Aromatic Hydrocarbons in Iranian Bread Samples. *Polycyclic Aromatic Compounds*, *40*(4), 1187-1195. https://doi.org/10.1080/10406638.2018.1534747

Kim, J. H., Nam, Y. P., Jeon, S. M., Han, H. S., & Suk, K. (2012). Amyloid neurotoxicity is attenuated by metallothionein: dual mechanisms at work. *Journal of Neurochemistry*, *121*(5), 751-762. https://doi.org/10.1111/j.1471-4159.2012.07725.x

Kirman, C. R., Gargas, M. L., Deskin, R., Tonner-Navarro, L., & Andersen, M. E. (2003). A physiologically based pharmacokinetic model for acrylamide and its metabolite, glycidamide, in the rat. *Journal of Toxicology and Environmental Health-Part a-Current Issues*, *66*(3), 253-274. https://doi.org/10.1080/15287390306368

Knafla, A., Phillipps, K. A., Brecher, R. W., Petrovic, S., & Richardson, M. (2006). Development of a dermal cancer slope factor for benzo[a]pyrene. *Regulatory Toxicology and Pharmacology*, *45*(2), 159-168. https://doi.org/10.1016/j.yrtph.2006.02.008

Kobayashi, E. H., Suzuki, T., Funayama, R., Nagashima, T., Hayashi, M., Sekine, H., Tanaka, N., Moriguchi, T., Motohashi, H., Nakayama, K., & Yamamoto, M. (2016). Nrf2 suppresses macrophage inflammatory response by blocking proinflammatory cytokine transcription. *Nature Communications*, *7*. https://doi.org/ARTN 11624
10.1038/ncomms11624

Kopanska, M., Lukac, N., Kapusta, E., & Formicki, G. (2015). Acrylamide Influence on Activity of Acetylcholinesterase, Thiol Groups, and Malondialdehyde Content in the Brain of Swiss Mice. *Journal of Biochemical and Molecular Toxicology*, *29*(10), 472-478. https://doi.org/10.1002/jbt.21717

Koszucka, A., Nowak, A., Nowak, I., & Motyl, I. (2020). Acrylamide in human diet, its metabolism, toxicity, inactivation and the associated European Union legal regulations in food industry. *Crit Rev Food Sci Nutr*, *60*(10), 1677-1692. https://doi.org/10.1080/10408398.2019.1588222

Kumagai, Y., & Abiko, Y. (2017). Environmental Electrophiles: Protein Adducts, Modulation of Redox Signaling, and Interaction with Persulfides/Polysulfides. *Chemical Research in Toxicology*, *30*(1), 203-219. https://doi.org/10.1021/acs.chemrestox.6b00326

Li, D. T., Wang, P. P., Liu, Y. B., Hu, X. S., & Chen, F. (2016). Metabolism of Acrylamide: Interindividual and Interspecies Differences as Well as the Application as Biomarkers. *Current Drug Metabolism*, *17*(4), 317-326. https://doi.org/10.2174/1389200216666151015115007

Li, R. J., Cheng, M. C., Cui, Y., He, Q. S., Guo, X. F., Chen, L. G., & Wang, X. M. (2020). Distribution of the Soil PAHs and Health Risk Influenced by Coal Usage Processes in Taiyuan City, Northern China. *International Journal of Environmental Research and Public Health*, *17*(17). https://doi.org/ARTN 6319
10.3390/ijerph17176319

Li, Y., Tan, M. S., Jiang, T., & Tan, L. (2014). Microglia in Alzheimer's Disease. *Biomed Research International*, *2014*. https://doi.org/Artn 437483
10.1155/2014/437483

Liddell, J. R., Hoepken, H. H., Crack, P. J., Robinson, S. R., & Dringen, R. (2006). Glutathione peroxidase 1 and glutathione are required to protect mouse astrocytes from iron-mediated hydrogen peroxide toxicity. *Journal of Neuroscience Research*, *84*(3), 578-586. https://doi.org/10.1002/jnr.20957

Lineback, D. R., Coughlin, J. R., & Stadler, R. H. (2012). Acrylamide in Foods: A Review of the Science and Future Considerations. *Annual Review of Food Science and Technology, Vol 3*, *3*, 15-35. https://doi.org/10.1146/annurev-food-022811-101114

Liu, D., Zhao, Y., Qi, Y., Gao, Y., Tu, D., Wang, Y., Gao, H. M., & Zhou, H. (2020). Benzo(a)pyrene exposure induced neuronal loss, plaque deposition, and cognitive decline in APP/PS1 mice. *J Neuroinflammation*, *17*(1), 258. https://doi.org/10.1186/s12974-020-01925-y

Liu, Y., Zhang, X., Yan, D., Wang, Y., Wang, N., Liu, Y., Tan, A., Chen, X., & Yan, H. (2020). Chronic acrylamide exposure induced glia cell activation, NLRP3 infl-ammasome upregulation and cognitive impairment. *Toxicol Appl Pharmacol*, *393*, 114949. https://doi.org/10.1016/j.taap.2020.114949

LoPachin, R. M., Barber, D. S., He, D., & Das, S. (2006). Acrylamide inhibits dopamine uptake in rat striatal synaptic vesicles. *Toxicological Sciences*, *89*(1), 224-234. https://doi.org/10.1093/toxsci/kfj005

LuX. (2014). Research progress of acrylamide in cosmetics and its detection. *China Med Pharm*, *4*, 52–55.

Lynch, M. A. (2004). Long-term potentiation and memory. *Physiol Rev*, *84*(1), 87-136. https://doi.org/10.1152/physrev.00014.2003

M.Törnqvist. (2005). Acrylamide in food: the discovery and its implications: a historical perspective. *Adv Exp Med Biol*, *561*, 1-19.

Maciel, E. S., Biasibetti, R., Costa, A. P., Lunardi, P., Schunck, R. V., Becker, G. C., Arbo, M. D., Dallegrave, E., Goncalves, C. A., Saldiva, P. H., Garcia, S. C., Leal, R. B., & Leal, M. B. (2014). Subchronic oral administration of Benzo[a]pyrene impairs motor and cognitive behavior and modulates S100B levels and MAPKs in rats. *Neurochemical Research*, *39*(4), 731-740. https://doi.org/10.1007/s11064-014-1261-y

Mangiarini, L., Sathasivam, K., Seller, M., Cozens, B., Harper, A., Hetherington, C., Lawton, M., Trottier, Y., Lehrach, H., Davies, S. W., & Bates, G. P. (1996). Exon 1 of the HD gene with an expanded CAG repeat is sufficient to cause a progressive neurological phenotype in transgenic mice. *Cell*, *87*(3), 493-506. https://doi.org/Doi 10.1016/S0092-8674(00)81369-0

Mason, J. L., Suzuki, K., Chaplin, D. D., & Matsushima, G. K. (2001). Interleukin-1beta promotes repair of the CNS. *Journal of Neuroscience*, *21*(18), 7046-7052. https://www.ncbi.nlm.nih.gov/pubmed/11549714

Merrill, J. E., & Benveniste, E. N. (1996). Cytokines in inflammatory brain lesions: helpful and harmful. *Trends in Neurosciences*, *19*(8), 331-338. https://doi.org/10.1016/0166-2236(96)10047-3

Mezzaroma, E., Toldo, S., Farkas, D., Seropian, I. M., Van Tassell, B. W., Salloum, F. N., Kannan, H. R., Menna, A. C., Voelkel, N. F., & Abbate, A. (2011). The inflammasome promotes adverse cardiac remodeling following acute myocardial infarction in the mouse. *Proceedings of the National Academy of Sciences of the United States of America*, *108*(49), 19725-19730. https://doi.org/10.1073/pnas.1108586108

Migdal, W., Walczycka, M., & Migdal, L. (2022). The Levels of Polycyclic Aromatic Hydrocarbons in Traditionally Smoked Cheeses in Poland. *Polycyclic Aromatic Compounds*, *42*(4), 1391-1403. https://doi.org/10.1080/10406638.2020.1781207

Mitchell, J. R., Jollow, D. J., Potter, W. Z., Gillette, J. R., & Brodie, B. B. (1973). Acetaminophen-induced hepatic necrosis. IV. Protective role of glutathione. *J Pharmacol Exp Ther*, *187*(1), 211-217. https://www.ncbi.nlm.nih.gov/pubmed/4746329

Mohr, S., Stamler, J. S., & Brune, B. (1994). Mechanism of Covalent Modification of Glyceraldehyde-3-Phosphate Dehydrogenase at Its Active-Site Thiol by Nitric-Oxide, Peroxynitrite and Related Nitrosating Agents. *Febs Letters*, *348*(3), 223-227. https://doi.org/Doi 10.1016/0014-5793(94)00596-6

Mottram, D. S., Wedzicha, B. L., & Dodson, A. T. (2002). Acrylamide is formed in the Maillard reaction. *Nature*, *419*(6906), 448-449. https://doi.org/10.1038/419448a

Mucci, L. A., & Wilson, K. A. (2008). Acrylamide intake through diet and human cancer risk. *Journal of Agricultural and Food Chemistry*, *56*(15), 6013-6019. https://doi.org/10.1021/jf703747b

Niu, Q., Zhang, H., Li, X., & Li, M. (2010). Benzo[a]pyrene-induced neurobehavioral function and neurotransmitter alterations in coke oven workers. *Occup Environ Med*, *67*(7), 444-448. https://doi.org/10.1136/oem.2009.047969

Ny, E. T., Heederik, D., Kromhout, H., & Jongeneelen, F. (1993). The Relationship between Polycyclic Aromatic-Hydrocarbons in Air and in Urine of Workers in a Soderberg Potroom. *American Industrial Hygiene Association Journal*, *54*(6), 277-284. https://doi.org/Doi 10.1202/0002-8894(1993)054<0277:Trbpah>2.0.Co;2

Patil, S. P., Jain, P. D., Sancheti, J. S., Ghumatkar, P. J., Tambe, R., & Sathaye, S. (2014). RETRACTED: Neuroprotective and neurotrophic effects of Apigenin and Luteolin in MPTP induced parkinsonism in mice. *Neuropharmacology*, *86*, 192-202. https://doi.org/10.1016/j.neuropharm.2014.07.012

Paxinos , G., & Franklin, K. B. J. E. (2004). The Mouse Brain in Stereotaxic Coordinates,2nded. *ElsevierAcademicPress*.

Pennisi, M., Malaguarnera, G., Puglisi, V., Vinciguerra, L., Vacante, M., & Malaguarnera, M. (2013). Neurotoxicity of Acrylamide in Exposed Workers. *International Journal of Environmental Research and Public Health*, *10*(9), 3843-3854. https://doi.org/10.3390/ijerph10093843

Qiu, C., Cheng, S., Xia, Y., Peng, B., Tang, Q., & Tu, B. (2011). Effects of subchronic benzo(a)pyrene exposure on neurotransmitter receptor gene expression in the rat hippocampus related with spatial learning and memory change. *Toxicology*, *289*(2-3), 83-90. https://doi.org/10.1016/j.tox.2011.07.012

Qiu, C., Peng, B., Cheng, S., Xia, Y., & Tu, B. (2013). The effect of occupational exposure to benzo[a]pyrene on neurobehavioral function in coke oven workers. *Am J Ind Med*, *56*(3), 347-355. https://doi.org/10.1002/ajim.22119

Ramadoss, P., Marcus, C., & Perdew, G. H. (2005). Role of the aryl hydrocarbon receptor in drug metabolism. *Expert Opin Drug Metab Toxicol*, *1*(1), 9-21. https://doi.org/10.1517/17425255.1.1.9

Report, E., (B[a]P), E. A. B. a. P., & Mapping., A. (2021). Benzo(a)pyrene (BaP) annual mapping—Eionet. Available online: https://www.eionet.europa.eu (accessed on 12 May 2022).

Rifai, L., & Saleh, F. A. (2020). A Review on Acrylamide in Food: Occurrence, Toxicity, and Mitigation Strategies. *Int J Toxicol*, *39*(2), 93-102. https://doi.org/10.1177/1091581820902405

Rojo, A. I., Sagarra, M. R., & Cuadrado, A. (2008). GSK-3beta down-regulates the transcription factor Nrf2 after oxidant damage: relevance to exposure of neuronal cells to oxidative stress. *Journal of Neurochemistry*, *105*(1), 192-202. https://doi.org/10.1111/j.1471-4159.2007.05124.x

Rotshenker, S., Aamar, S., & Barak, V. (1992). Interleukin-1 Activity in Lesioned Peripheral-Nerve. *Journal of Neuroimmunology*, *39*(1-2), 75-80. https://doi.org/Doi 10.1016/0165-5728(92)90176-L

Ruben, J., Schwiemann, J., Deuchert, M., Meyer, R., Krause, T., Curio, G., Villringer, K., Kurth, R., & Villringer, A. (2001). Somatotopic organization of human secondary somatosensory cortex. *Cerebral Cortex*, *11*(5), 463-473. https://doi.org/DOI 10.1093/cercor/11.5.463

Ruenz, M., Bakuradze, T., Eisenbrand, G., & Richling, E. (2016). Monitoring urinary mercapturic acids as biomarkers of human dietary exposure to acrylamide in combination

with acrylamide uptake assessment based on duplicate diets. *Archives of Toxicology*, *90*(4), 873-881. https://doi.org/10.1007/s00204-015-1494-9

Sampaio, G. R., Guizellini, G. M., da Silva, S. A., de Almeida, A. P., Pinaffi-Langley, A. C. C., Rogero, M. M., de Camargo, A. C., & Torres, E. A. F. S. (2021). Polycyclic Aromatic Hydrocarbons in Foods: Biological Effects, Legislation, Occurrence, Analytical Methods, and Strategies to Reduce Their Formation. *International Journal of Molecular Sciences*, *22*(11). https://doi.org/ARTN 6010
10.3390/ijms22116010

Santonicola, S., Albrizio, S., Murru, N., Ferrante, M. C., & Mercogliano, R. (2017). Study on the occurrence of polycyclic aromatic hydrocarbons in milk and meat/fish based baby food available in Italy. *Chemosphere*, *184*, 467-472. https://doi.org/10.1016/j.chemosphere.2017.06.017

Saunders, C. R., Das, S. K., Ramesh, A., Shockley, D. C., & Mukherjee, S. (2006). Benzo(a)pyrene-induced acute neurotoxicity in the F-344 rat: role of oxidative stress. *J Appl Toxicol*, *26*(5), 427-438. https://doi.org/10.1002/jat.1157

Schneider , C. A., Rasband, W. S., & Eliceiri, K. W. (2012). NIH Image to ImageJ: 25years of image analysis. *Nature Methods*, *9*, 671–675.

Sehsah, R., Wu, W. T., Ichihara, S., Hashimoto, N., Hasegawa, Y., Zong, C., Itoh, K., Yamamoto, M., Elsayed, A. A., El-Bestar, S., Kamel, E., & Ichihara, G. (2019). Role of Nrf2 in inflammatory response in lung of mice exposed to zinc oxide nanoparticles. *Particle and Fibre Toxicology*, *16*(1). https://doi.org/ARTN 47
10.1186/s12989-019-0328-y

Sen, S., Narayana, J., Ravichandran, B., & Dhananjayan, V. (2018). Polyaromatic Hydrocarbons Depositions and Their Carcinogenic Risk Assessment in the Foundry Workers. *Aerosol Science and Engineering*, *2*(4), 173-181. https://doi.org/10.1007/s41810-018-0034-4

Shanmugam, G., Narasimhan, M., Tamowski, S., Darley-Usmar, V., & Rajasekaran, N. S. (2017). Constitutive activation of Nrf2 induces a stable reductive state in the mouse myocardium. *Redox Biology*, *12*, 937-945. https://doi.org/10.1016/j.redox.2017.04.038

Sloan, S. A., & Barres, B. A. (2014). Mechanisms of astrocyte development and their contributions to neurodevelopmental disorders. *Current Opinion in Neurobiology*, *27*, 75-81. https://doi.org/10.1016/j.conb.2014.03.005

Smith, E. A., Prues, S. L., & Oehme, F. W. (1997). Environmental degradation of polyacrylamides .2. Effects of environmental (outdoor) exposure. *Ecotoxicology and Environmental Safety*, *37*(1), 76-91. https://doi.org/DOI 10.1006/eesa.1997.1527

Sofroniew, M. V., & Vinters, H. V. (2010). Astrocytes: biology and pathology. *Acta Neuropathologica*, *119*(1), 7-35. https://doi.org/10.1007/s00401-009-0619-8

Spencer, P. S., & Schaumburg, H. H. (1974). A review of acrylamide neurotoxicity. Part II. Experimental animal neurotoxicity and pathologic mechanisms. *CJNS*, *1*(3), 152-169. https://doi.org/10.1017/s0317167100119201

Spencer, P. S., & Schaumburg, H. H. (1975). Nervous system degeneration produced by acrylamide monomer. *Environ Health Perspect*, *11*, 129-133. https://doi.org/10.1289/ehp.7511129

Stephanou, P., Konstandi, M., Pappas, P., & Marselos, M. (1998). Alterations in central monoaminergic neurotransmission induced by polycyclic aromatic hydrocarbons in rats. *Eur J Drug Metab Pharmacokinet*, *23*(4), 475-481. https://doi.org/10.1007/BF03189998

Streit, W. J., Graeber, M. B., & Kreutzberg, G. W. (1988). Functional Plasticity of Microglia - a Review. *Glia*, *1*(5), 301-307. https://doi.org/DOI 10.1002/glia.440010502

Streit, W. J., & Xue, Q. S. (2009). Life and Death of Microglia. *Journal of Neuroimmune Pharmacology*, *4*(4), 371-379. https://doi.org/10.1007/s11481-009-9163-5

Strobel, H. W., Thompson, C. M., & Antonovic, L. (2001). Cytochromes P450 in brain: function and significance. *Current Drug Metabolism*, *2*(2), 199-214. https://doi.org/10.2174/1389200013338577

Takahashi, E., Niimi, K., & Itakura, C. (2009). Motor coordination impairment in aged heterozygous rolling Nagoya, Cav2.1 mutant mice. *Brain Research*, *1279*, 50-57. https://doi.org/10.1016/j.brainres.2009.05.016

Tareke, E., Rydberg, P., Karlsson, P., Eriksson, S., & Tornqvist, M. (2000). Acrylamide: a cooking carcinogen? *Chem Res Toxicol*, *13*(6), 517-522. https://doi.org/10.1021/tx9901938

Tareke, E., Rydberg, P., Karlsson, P., Eriksson, S., & Tornqvist, M. (2002). Analysis of acrylamide, a carcinogen formed in heated foodstuffs. *Journal of Agricultural and Food Chemistry*, *50*(17), 4998-5006. https://doi.org/10.1021/jf020302f

Tschopp, J., & Schroder, K. (2010). NLRP3 inflammasome activation: The convergence of multiple signalling pathways on ROS production? *Nat Rev Immunol*, *10*(3), 210-215. https://doi.org/10.1038/nri2725

Tu, B., Wu, T., & He, H. (2004). [Study on the neurotoxicity and brain tissue HSPs level in benzo[a]pyrene exposed mice]. *Wei Sheng Yan Jiu*, *33*(1), 15-17. https://www.ncbi.nlm.nih.gov/pubmed/15098469

Varallyay, C. G., Nesbit, E., Fu, R., Gahramanov, S., Moloney, B., Earl, E., Muldoon, L. L., Li, X., Rooney, W. D., & Neuwelt, E. A. (2013). High-resolution steady-state cerebral blood volume maps in patients with central nervous system neoplasms using ferumoxytol, a superparamagnetic iron oxide nanoparticle. *J Cereb Blood Flow Metab*, *33*(5), 780-786. https://doi.org/10.1038/jcbfm.2013.36

Viswanath, P. (2012). Evaluation of certain contaminants in food.In: Proceedings of the 72nd Report of the Joint FAO/WHO Expert Committee on Food Additives. *Geneva: Medknow Publications and Media Pvt. Ltd*.

Von Burg, R., Penney, D. P., & Conroy, P. J. (1981). Acrylamide neurotoxicity in the mouse: a behavioral, electrophysiological and morphological study. *J Appl Toxicol*, *1*(4), 227-233. https://doi.org/10.1002/jat.2550010409

Wang, H., Ichihara, G., Ito, H., Kato, K., Kitoh, J., Yamada, T., Yu, X., Tsuboi, S., Moriyama, Y., Sakatani, R., Shibata, E., Kamijima, M., Itohara, S., & Takeuchi, Y. (2002). Biochemical changes in the central nervous system of rats exposed to 1-bromopropane for seven days. *Toxicol Sci*, *67*(1), 114-120. https://doi.org/10.1093/toxsci/67.1.114

Wang, H., Ichihara, G., Ito, H., Kato, K., Kitoh, J., Yamada, T., Yu, X., Tsuboi, S., Moriyama, Y., & Takeuchi, Y. (2003). Dose-dependent biochemical changes in rat central nervous system after 12-week exposure to 1-bromopropane. *Neurotoxicology*, *24*(2), 199-206. https://doi.org/10.1016/S0161-813X(02)00195-X

Wang, H. Y., Wang, C., Li, C. B., Xu, X. L., & Zhou, G. H. (2019). Effects of Phenolic Acid Marinades on the Formation of Polycyclic Aromatic Hydrocarbons in Charcoal-Grilled Chicken Wings. *Journal of Food Protection*, *82*(4), 684-690. https://doi.org/10.4315/0362-028x.Jfp-18-420

WHO. (2011). EVALUATION OF CERTAIN CONTAMINANTS IN FOOD Introduction. *Evaluation of Certain Contaminants in Food*, *959*, 1-+. <Go to ISI>://WOS:000291953900001

Wong, J. Y. Y., Hu, W., Downward, G. S., Seow, W. J., Bassig, B. A., Ji, B. T., Wei, F., Wu, G., Li, J., He, J., Liu, C. S., Cheng, W. L., Huang, Y., Yang, K., Chen, Y., Rothman, N., Vermeulen, R. C., & Lan, Q. (2017). Personal exposure to fine particulate matter and benzo[a]pyrene from indoor air pollution and leukocyte mitochondrial DNA copy number in rural China. *Carcinogenesis*, *38*(9), 893-899. https://doi.org/10.1093/carcin/bgx068

Wu Ruoyu, B. C., Xiang Jia, Yu Qiu, Mengyu Liu,Chengsheng Huang, Jie Feng and Qingkai Wu. (2018). Interleukin-1b influences functional regeneration following nerve injury in mice through nuclear factor-jB signaling pathway. . *Immunology*, *156*, 235–248

Wu, W., Ichihara, G., Suzuki, Y., Izuoka, K., Oikawa-Tada, S., Chang, J., Sakai, K., Miyazawa, K., Porter, D., Castranova, V., Kawaguchi, M., & Ichihara, S. (2014). Dispersion method for safety research on manufactured nanomaterials. *Ind Health*, *52*(1), 54-65. https://doi.org/10.2486/indhealth.2012-0218

Xia, Y., Cheng, S., He, J., Liu, X., Tang, Y., Yuan, H., He, L., Lu, T., Tu, B., & Wang, Y. (2011). Effects of subchronic exposure to benzo[a]pyrene (B[a]P) on learning and memory, and neurotransmitters in male Sprague-Dawley rat. *Neurotoxicology*, *32*(2), 188-198. https://doi.org/10.1016/j.neuro.2010.12.015

Yang, S. K., McCourt, D. W., Leutz, J. C., & Gelboin, H. V. (1977). Benzo[a]pyrene diol epoxides: mechanism of enzymatic formation and optically active intermediates. *Science*, *196*(4295), 1199-1201. https://doi.org/10.1126/science.870975

Yousef, M. I., & El-Demerdash, F. M. (2006). Acrylamide-induced oxidative stress and biochemical perturbations in rats. *Toxicology*, *219*(1-3), 133-141. https://doi.org/10.1016/j.tox.2005.11.008

Zhang, H., Nie, J., Li, X., & Niu, Q. (2013). Association of aryl hydrocarbon receptor gene polymorphism with the neurobehavioral function and autonomic nervous system function changes induced by benzo[a]pyrene exposure in coke oven workers. *J Occup Environ Med*, *55*(3), 265-271. https://doi.org/10.1097/JOM.0b013e318278272f

Zhang, H. M., Nie, J. S., Wang, F., Shi, Y. T., Zhang, L., Antonucci, A., Liu, H. J., Wang, J., Zhao, J., Zhang, Q. L., Wang, L. P., Song, J., Xue, C. E., Di Gioacchino, M., & Niu, Q. (2008). Effects of benzo[a]pyrene on autonomic nervous system of coke oven workers. *J Occup Health*, *50*(4), 308-316. https://doi.org/10.1539/joh.l7155

Zhang, Y., Wang, Q., Zhang, G., Jia, W., Ren, Y. P., & Wu, Y. N. (2018). Biomarker analysis of hemoglobin adducts of acrylamide and glycidamide enantiomers for mid-term internal exposure assessment by isotope dilution ultra-high performance liquid chromatography tandem mass spectrometry. *Talanta*, *178*, 825-833. https://doi.org/10.1016/j.talanta.2017.09.092

Zhao, M., Lewis Wang, F. S., Hu, X., Chen, F., & Chan, H. M. (2017). Acrylamide-induced neurotoxicity in primary astrocytes and microglia: Roles of the Nrf2-ARE and NF-kappaB pathways. *Food Chem Toxicol*, *106*(Pt A), 25-35. https://doi.org/10.1016/j.fct.2017.05.007

Zong, C., Hasegawa, R., Urushitani, M., Zhang, L. Y., Nagashima, D., Sakurai, T., Ichihara, S., Ohsako, S., & Ichihara, G. (2019). Role of microglial activation and neuroinflammation

in neurotoxicity of acrylamide in vivo and in vitro. *Archives of Toxicology*, *93*(7), 2007-2019. https://doi.org/10.1007/s00204-019-02471-0

Zong, C., Hasegawa, R., Urushitani, M., Zhang, L. Y., Nagashima, D., Sakurai, T., Ichihara, S., Ohsako, S., & Ichihara, G. (2019). Role of microglial activation and neuroinflammation in neurotoxicity of acrylamide in vivo and in vitro. *Archives of Toxicology*, *93*(7), 2007-2019. https://doi.org/10.1007/s00204-019-02471-0